An improved global land cover mapping in 2015 with 30 m resolution (GLC-2015) based on a multi-source product fusion approach

Bingjie Li [1], Xiaocong Xu [1], Xiaoping Liu [1 2], Qian Shi [1], Haoming Zhuang [1], Yaotong Cai [1] and Da He [1]

[1]School of Geography and Planning, Sun Yat-Sen University, Guangzhou, 510275, China

[2]Southern Marine Science and Engineering Guangdong Laboratory (Zhuhai), Zhuhai, 519080, China

Correspondence to: Xiaoping Liu (liuxp3@mail.sysu.edu.cn)

Abstract. Global land cover (GLC) information with fine spatial resolution is a fundamental data input for studies on biogeochemical cycles of the Earth system and global climate change. Although there are several public GLC products with 30 m resolution, considerable inconsistencies were found among them especially in fragmented regions and transition zones, which brings great uncertainties to various application tasks. In this paper, we developed an improved global land cover map in 2015 with 30 m resolution (GLC-2015) by fusing multiple existing land cover products based on the Dempster-Shafer theory of evidence (DSET). Firstly, we used more than 160,000 global point-based samples to locally evaluated the reliability of the input GLC products for each LC class within each 4°×4° geographical grid for the establishment of the basic probability assignment (BPA) function. Then, the Dempster's rule of combination was used for each 30 m pixel to derive the combined probability mass of each possible land cover class from all the candidate maps. Finally, each pixel was determined with a land cover class based on a decision rule. Through this fusing process, each pixel is expected to be assigned with the land cover class that contributes to achieve a higher accuracy. We assessed our product separately with 34,987 global point-based samples and 201 global patch-based samples. Results show that, the GLC-2015 map achieved the highest mapping performance globally, continentally, and eco-regionally compared with the existing 30 m GLC maps, with an overall accuracy of 76.0% (84.4%) and a kappa coefficient of 0.715 (0.564) against the point-based (patch-based) validation samples. Additionally, we found that the GLC-2015 map showed substantial outperformance in the areas of inconsistency, with an accuracy

27 improvement of 17.6%-23.2% in areas of moderate inconsistency, and 21.0%-25.2% in areas of high

28 inconsistency. Hopefully, this improved GLC-2015 product can be applied to reduce uncertainties in the

29 research on global environmental changes, ecosystem service assessments, and hazard damage

30 evaluations, etc. The GLC-2015 map developed in this study is available at

31 https://doi.org/10.6084/m9.figshare.21371304.v1 (Li et al., 2022).

32 **1. Introduction**

33 Land cover (LC), influenced by both nature and human activities (Running, 2008; Gong et al., 2013;

34 Song et al., 2018; Liu et al., 2021a), is a significant component of the Earth system (Yang and Huang,

35 2021). Global land cover (GLC) products can serve as fundamental data for various studies, such as

36 climate and environmental changes (Bounoua et al., 2002; Foley et al., 2005; Grimm et al., 2008; Yang

37 et al., 2013; Schewe et al., 2019), food security (Verburg et al., 2013; Ban et al., 2015), carbon cycling

38 (Moody and Woodcock, 1994; Defries et al., 2002; Gómez et al., 2016), biodiversity conservation

39 (Chapin et al., 2000; Giri et al., 2005) and land management (Mayaux et al., 2004; Verburg et al., 2011).

40 Therefore, there is a pressing need for detailed, accurate, and high-quality GLC product to support global

41 change research and sustainable development.

42   In the preliminary stage, LC mapping mainly relied on visual interpretation, which is time-

43 consuming, labor-intensive and difficult to be applied at the global scale (Gong, 2012). In recent decades,

44 satellite remote sensing data, which can provide information of large area coverage and long-term

45 monitoring, has been adopted to generate GLC products. With coarse resolution satellite data such as

46 Advanced Very High Resolution Radiometer (AVHRR), Moderate Resolution Imaging

47 Spectroradiometer (MODIS), Medium Resolution Imaging Spectrometer (MERIS), and Global Land

48 Surface Satellite (GLASS), a variety of GLC products have been developed at 5 km to 300 m

49 resolution(Loveland et al., 2000; Hansen et al., 2000; Bartholomé and Belward, 2005; Friedl et al., 2010;

50 Defourny et al., 2018; Liu et al., 2020a). Although these GLC products have been widely applied to many

51 applications, it has been proved that the differences between sensors, classification systems, and

52 considerably low accuracies in areas prevent harmonization of these products (Herold et al., 2008;

53 Verburg et al., 2011; Grekousis et al., 2015). Also, these products are far from providing enough fine

54 spatial details of LC due to their relatively coarse spatial resolution, which does not meet the demand of

55　　many studies (Giri et al., 2013; Yang et al., 2017). To allow researches which can capture most human

56　　activity, finer-resolution (e.g., 30 m) GLC products are demanded (Giri et al., 2013).

57　　　　With the free accessibility of high-resolution satellite remote sensing data, GLC mapping at fine

58　　resolution has been successfully conducted. Using Landsat imagery, there has been a milestone

59　　achievement that the two GLC products are generated with fine resolution of 30 m, namely Finer

60　　Resolution Observation and Monitoring of Global Land Cover product (FROM_GLC)(Gong et al.,

61　　2013)and Globeland30 (Chen et al., 2015). After that, a 30 m-resolution GLC mapping in 2017 was

62　　achieved using the first all-season sample set (Li et al., 2017). More recently, Zhang et al. (2021) used

63　　both Landsat time series imagery and high-quality training data from the Global Spatial Temporal Spectra

64　　Library (GSPECLib) to produce a 30 m GLC map in 2015 (GLC_FCS30) with a two-level classification

65　　scheme. Several attempts have been made to improve accuracy of 30 m GLC products which are

66　　prevail in the generation of GLC mapping task over the last few years. FROM_GLC was created by

67　　employing four classification algorithms to classify the Landsat images and choosing time series of

68　　MODIS EVI data for training and test. Globeland30 was created by proposing a pixel-object-knowledge-

69　　based (POK) method to assure consistency and accuracy. GLC_FCS30 was generated by adopting local

70　　adaptive random forest models with high-quality training samples derived from GSPECLib.

71　　　　Despite the great efforts in producing more accurate products, the existing 30 m GLC products still

72　　show low accuracy performance in certain LC classes and some specific areas (Sun et al., 2016; Kang et

73　　al., 2020). Furthermore, the existing 30 m products showed great agreement in overall spatial distribution

74　　patterns but significant spatial inconsistency in some specific areas (heterogeneous areas and transition

75　　zones) and spectrally similar classes (forest and shrubland, cropland and grassland) (Gao et al., 2020;

76　　Liu et al., 2021b). The high spatial inconsistency between the existing 30m GLC products are resulted

77　　from differences in their classification systems, classification techniques employed, source data, and

78　　spatial distribution and size of training samples (Yang et al., 2017; Gao et al., 2020). Due to the aforesaid

79　　limitations, users of GLC products still have difficulties in an appropriate selection of data for their

80　　specific application. Ultimately, this situation leads to uncertainties in outcomes of related researches

81　　when different 30 m GLC products are used. For GLC mapping with fine spatial resolution, more efforts

82　　should be focused on improving the mapping in heterogenous and fragmented landscape (Herold et al.,

83　　2008; Liu et al., 2021b). Therefore, it is pressing to generate a more accurate and reliable GLC product

84   with high classification accuracy, especially for spatially inconsistent regions and low-accuracy LC

85   classes.

86   According to Gong et al. (2016), inconsistencies between LC products indicate available

87   complementary information and more robust and reliable data can be generated by integrating the input

88   maps with the data fusion method. Given that different maps have disagreement and provide accurate

89   information in different locations, we can make a best choice for the class label assigned to each pixel

90   by weighting the credibility of all the available information and combining them through a decision rule

91   (Clinton et al., 2015). In this way, the output map of integration on input maps can reduce the overall risk

92   of assigning a wrong class label to a pixel and at least achieve the average performance of input maps.

93   Several attempts have been made to produce an accurate and consistent LC map using various methods,

94   such as majority voting (MV), fuzzy agreement and Bayesian theory. Iwao et al. (2011) created a GLC

95   map based on a simple majority voting method. Jung et al. (2006) generated a 1km GLC map by

96   combination of MODIS, GLC2000 and GLCC data based on fuzzy agreement scoring. Subsequently,

97   Fritz et al. (2011) extended the synergy method of Jung et al. (2006) by ranking LC maps and mapped

98   the cropland extent in Sub-Saharan Africa. See et al. (2015) generated two GLC products by integrating

99   medium resolution LC products with geographically weighted regression (GWR). Gengler and Bogaert

100   (2018) proposed a Bayesian data fusion method and applied it to the LC mapping for a specific region in

101   Belgium. All these researches have demonstrated that fusion method can create an integrated LC product

102   where the mapping accuracy is greatly improved by combing the best of candidate maps. However, the

103   MV method is sensitive to the quality of the candidate maps and has significant uncertainties when the

104   input products exhibit great disagreement(Chen and Venkataramanan, 2005). The fuzzy agreement is

105   highly subjective since it depends on expert assessment, while the Bayesian theory requires a prior

106   knowledge or conditional probabilities and fails to handle the states of ignorance(Liu and Xu, 2021).

107   The Dempster-Shafer theory of evidence (DSET) is an evidence-based approach to reason with

108   uncertainties. Unlike the majority voting, the DSET method can discount evidence form inaccurate

109   information with a probability mass that reflects the degree of belief rather than a binary decision (Razi

110   et al., 2019). In contrast to the Bayesian theory, the DSET can integrate evidence from a variety of sources

111   without the requirement of prior knowledge (Chen and Venkataramanan, 2005). Moreover, the reliability

112   of the final fused results is measured the DSET method with a total degree of belief. Although previous

literature focused on the application of the DSET method in multisource data aggregation, very little research has been conducted at a global scale due to the lack of accurate and sufficient samples and the demand for adequate computing resources.

In this research, we propose a multi-source product fusion approach on the Google Earth Engine (GEE) platform to produce an improved GLC product in 2015 (GLC-2015) with 30 m resolution. The fusion approach we proposed aims to deal with the inconsistency between previous 30 m GLC products and generate a map which has better mapping performance than any of the candidate maps by evaluating the mapping accuracy of these existing products at the local scale and choosing the most credible LC class. To fulfill the purpose, we first performed reliability evaluation, where the accuracy of each GLC product for each LC class in each $4° \times 4°$ geographical grid is regarded as the evidential probability to create the basic probability assignment (BPA) function. Then, the BPA values of all the LC classes from different GLC products are fused according to the Dempster's rule of combination. Finally, the GLC-2015 map was integrated after a final accepted LC class with the maximum combined probability mass was assigned to each 30 m pixel. Our GLC-2015 map was separately validated with two different validation sets, namely global point-based samples and global patch-based samples, and compared with three existing multiple-class GLC products. Moreover, we provided an analysis for mapping improvement of the GLC-2015 compared to other products in areas of high mapping inconsistency. The GLC-2015 map is proved to be accurate and credible and can significantly improve the mapping accuracy in areas of high inconsistency between previous products.

2. Datasets

2.1 Multiple-class GLC products

Three existing 30m GLC products with multiple classes, including GlobeLand30, FROM_GLC and GLC_FCS30, were employed as input maps in the fusion based on DSET. A summary of their detailed information is shown in Table 1.

GlobeLand30, a widely-used global geo-information product, was produced by the POK-based method using Landsat and HJ-1 satellite images. Globeland30 products are freely accessible online at the website (http://www.globalland30.org) for 2000 and 2010. From the accuracy assessment, the Globeland30 for the year 2010 had an overall accuracy excessed 80% using large samples (Chen et al.,

2015). We employed the version of 2010 as one of the candidate maps for the mapping procedure.

FROM_GLC was first generated using numerous Landsat images, which has a fine classification system with a two-level structure. It achieved an OA of 64.5% through validation with the complete test samples and 71.5% with a subset of test samples in homogeneous areas (Gong et al., 2013). We used the version of 2015 for the fusion.

GLC_FCS30 was developed using Landsat time series data and large training samples from the GSPECLib. It has a two-level classification scheme that contains 16 global LCCS LC classes and 14 detailed regional LC classes. The overall accuracy of the GLC_FCS30 according to LCCS level-1 validation scheme reached 71.4% (Zhang et al., 2021).

Although the data time of GlobeLand30 is 2010, which has a five-year gap with other products, it was used in our project for the following reasons: (1) The changed areas of LC caused by the time interval are tiny compared to the global land area. In addition, there is relatively less uncertainty due to LC changes than due to inaccurate classification (Xu et al., 2014). Most spatial disagreements between the existing maps are about classification errors rather than LC changes over the time interval (Mccallum et al., 2006; See et al., 2015); (2) We used a global point-based sample set for the year 2015 to evaluate the reliability of the input products in all 4° × 4° grids. At locations where land cover changed between 2010 and 2015, the Globeland30 was more likely to have low accuracy based on the validation and less likely to contribute to the fusion using the DSET approach. In this way, the errors due to land cover changes can be largely avoided; (3) The GlobeLand30 has great popularity due to its good accuracy. The classification system of the GlobeLand30 is almost the same as that in our study.

Table 1. Detailed information of GLC products used in this paper.

Product name	Satellite sensors	Year of reference	Access	Literature
Globeland30	Landsat TM/ETM+ HJ-1 A/B	2010	http://www.globallandcover.com/	(Chen et al., 2015)
FROM_GLC	Landsat TM/ETM+/OLI	2015	http://data.ess.tsinghua.edu.cn/	(Gong et al., 2013)
GLC_FCS30	Landsat OLI	2015	https://doi.org/10.5281/zenodo.3986872	(Zhang et al., 2021)
GAUD	Landsat TM/ETM+/OLI	2015	https://doi.org/10.6084/m9.figshare.11513178.v1	(Liu et al., 2020b)
GFC	Landsat TM/ETM+	2015	http://earthenginepartners.appspot.com/science-2013-global-forest	(Hansen et al., 2013)

JRC GSW	Landsat TM/ETM+/OLI	2015	http://global-surface-water.appspot.com/	(Pekel et al., 2016)
GMW	ALOS PALSAR Landsat TM/ETM+	2015	https://data.unep-wcmc.org/datasets/45	(Bunting et al., 2018)

2.2 Single-class GLC products

To improve the quality of the fusing result, a set of highly qualified GLC products with single class at 30 m fine resolution were also used. Compared to the multiple-class GLC products, these single-class GLC products are more likely to provide accurate information since they usually focus on promoting mapping performance of specific LC class. These products include Global Forest Change (GFC) (Hansen et al., 2013), Global Annual Urban Dynamics (GAUD) (Liu et al., 2020b), Joint Research Centre's Global Surface Water (JRC GSW) (Pekel et al., 2016), and Global Mangrove Watch (GMW) (Bunting et al., 2018). While these single-class products are either annual or multi-epoch, we only selected these products in the target year of 2015. The background information of these single-class products was considered as another land cover class (e.g., non-water) participating in the fusion. The accuracy of the background information was defaulted to 0 since it did not provide information about any of the other nine categories in our classification system. Table 1 also describes the information of these selected single-class GLC products.

GFC was resulted from a time-series analysis of growing season Landsat scenes, aiming to provide information about global tree cover extent, gain, and loss at a 30m spatial resolution. The accuracy assessment was performed at global and climate domain scales and the forest gain reached an overall accuracy of 99.6% and forest loss reached 99.7% across the globe (Hansen et al., 2013). Up to now, it has a temporary coverage from 2000 to 2020.

GAUD, which provides 30m annual urban extent for the time period of 1985 to 2015, was generated using numerous Landsat images with both data fusion approach and temporal segmentation approach on the GEE platform. Validation was conducted across different urban ecoregions and the globe by the product developer. The accuracies of mapping urbanized year are 76% for the period of 1985 to 2000 and 82% for the period of 2000 to 2015 at humid regions worldwide (Liu et al., 2020b).

JRC GSW dataset provides a monthly presentation of global surface water changes from 1984 to 2015 at a fine 30 m resolution. Expert systems, visual analytics and evidential reasoning were exploited

187   to detect water extent and changes. Based on 40,124 validation points over the globe and across the 32

188   years, commission accuracies were determined with overall accuracies of 99.45% (TM), 99.35% (ETM+)

189   and 99.54% (OLI) and omission accuracies were reflected in overall accuracies of 97.01% (TM), 95.79%

190   (ETM+) and 96.25%(OLI) (Pekel et al., 2016). We used the GSW Yearly Water Classification History

191   v1.1 in the GEE catalog. A single 'waterClass' band is present in each image that provides the water's

192   seasonality throughout the year with four types: no data, no water, seasonal water, and permanent water.

193   Since the seasonal water in GSW data is not as reliable as the permanent water (Meyer et al., 2020), we

194   selected permanent water bodies and excluded seasonal water bodies.

195   GMW dataset was produced as a resulted of the GMW initiative, which aims to provide consistent

196   information of mangrove extent. The global mangrove map in 2010 was generated as a baseline map

197   employing the Extremely Randomized Trees classifier to classify ALOS PALSAR and Landsat imagery.

198   Assessed by a total of 53,878 sample points globally, the overall accuracy of the baseline map reached

199   95.3% and the producer's accuracy achieved 94.0% (Bunting et al., 2018). Based on the baseline in 2010,

200   mangrove extent maps for six epochs between 1996 and 2016 have been established and annual change

201   monitoring from 2018 and onwards are undertaken.

202   **2.3 Global point-based and patch-based samples**

203   In this study, we collected two sets of global samples, namely the global point-based samples and the

204   global patch-based samples. To collect representative and sufficient samples efficiently, we divided the

205   world's terrestrial area into 4° × 4° geographical grids. A total of 1,507 grids are distributed evenly across

206   the globe, shown as Figure. 1.

207
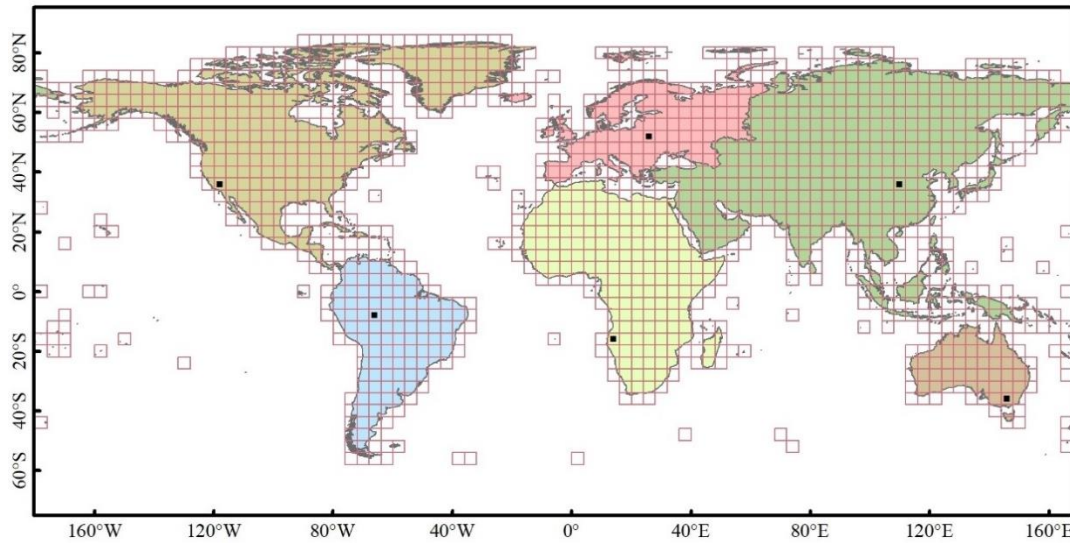
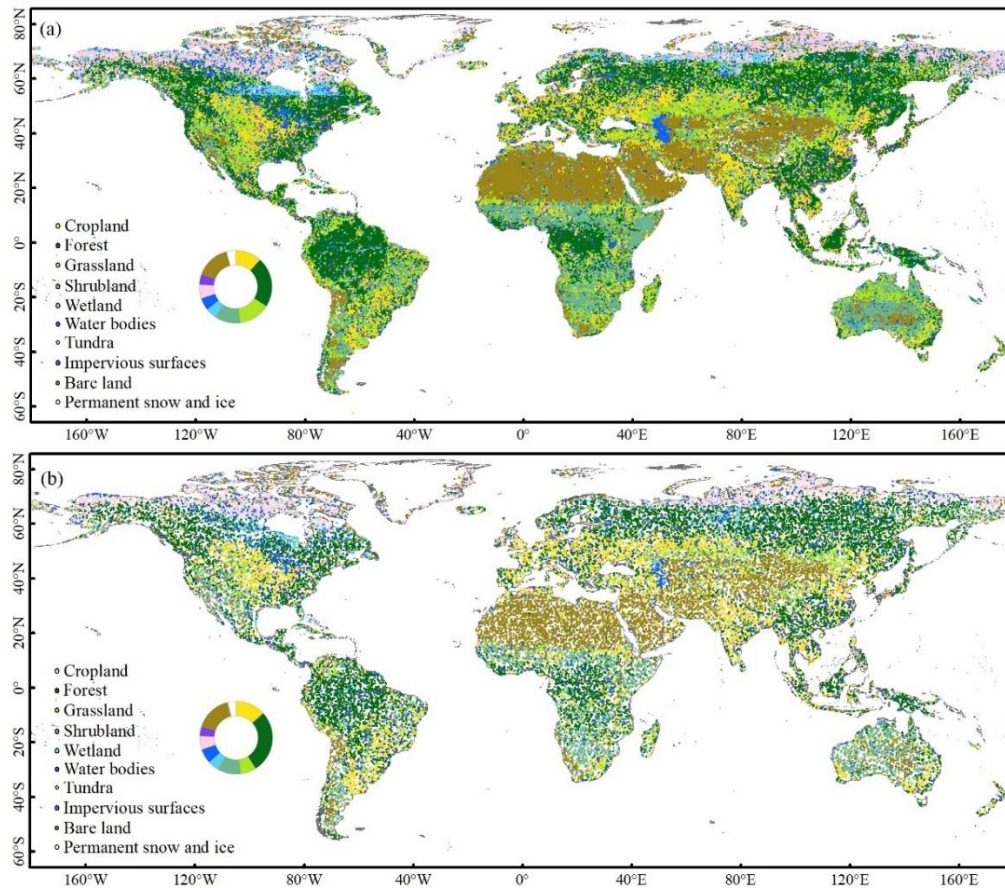**Figure 1. Spatial distribution of the 4° × 4° geographical grids over the world. Six black rectangle tiles with size of 0.25° were used for visual comparation between our product and other three products.**

To derive the global point-based samples, we adopted stratified random sampling in each grid. The stratified random sampling depends on area ratio of LC classes from a LC product. We used the FROM_GLC as prior knowledge rather than the Globeland30 and GLC_FCS30 with two considerations: (1) the FROM_GLC has the same data time as our target map (GLC-2015) while the Globeland30 has a 5-year interval from our samples, which affects the size of samples for each LC class; (2)the 10 level-1 land cover classes of the FROM_GLC is similar to that in the classification system of the GLC-2015, while the GLC_FCS30 has differences with the GLC-2015 in the classification scheme and definition of land cover classes. First, the FROM_GLC product was used to calculate the area ratio of each LC class. Then, points were randomly extracted from the FROM_GLC according to the area ratio and spatial location of each class. Finally, more than 200,000 global samples were collected. Through the sampling method mentioned above, the global point-based samples were even across the globe and sufficient for each LC class in each grid. Therefore, more than 50 points could be easily derived for LC classes with a small area ratio in the 4° × 4° grid. The FROM_GLC shows low accuracy for some LC classes, especially for cropland and forest (Gao et al., 2020; Liu et al., 2021b; Zhang et al., 2021; Zhang et al., 2022). If the global samples were extracted with LC class label from the FROM_GLC, there would be inevitable errors. Therefore, the FROM_GLC was only used to determine the size and location of samples for each LC class. Instead, all the points were manually labeled according to Google Earth high-resolution images. The whole sample set was randomly split into two subsets: 80% of the global samples were used to assess

9

228 the accuracy of each GLC product for various LC classes at the global scale and in each grid. The

229 remaining 20% were used for the validation of the GLC-2015 map and data inter-comparison between

230 different GLC products. Figure 2 presents the distribution of the whole global point-based samples and

231 the subset for accuracy assessment and data inter-comparison.

232
233 **Figure 2. Spatial distribution of (a) the global point-based samples, (b) the subset of the global point-based**
234 **samples for accuracy assessment and data inter-comparison, the proportions of each LC class are shown in**
235 **the pie chart.**

236   To verify the consistency between the GLC-2015 and the actual pattern of the landscape at the local

237 scale, we also established the global patch-based samples. Simple random sampling was used to derive

238 5 km × 5 km blocks over the world's terrestrial area and across different ecoregions because it is easy to

239 perform and capable to augment the sample size from target areas (Pengra et al., 2020). Since

240 inconsistency between current GLC maps tends to appear in those heterogeneous areas, such as

241 fragmented regions and transition zones, we slightly increased the sample size for areas with the

242 heterogeneous landscape to better evaluate our mapping results. In total, there were 201 blocks selected

243 as the global patch-based samples, as displayed in Figure. 3a. Then, for each block in the patch-based

244   samples, we used ArcGIS 10.5 software to derive polygons (patches) of various sizes which captured the

245   real landscape on the high-resolution images. Meanwhile, each polygon was manually labeled with a LC

246   class. Four examples of producing patch-based samples are shown in Figure. 3b-c.

247
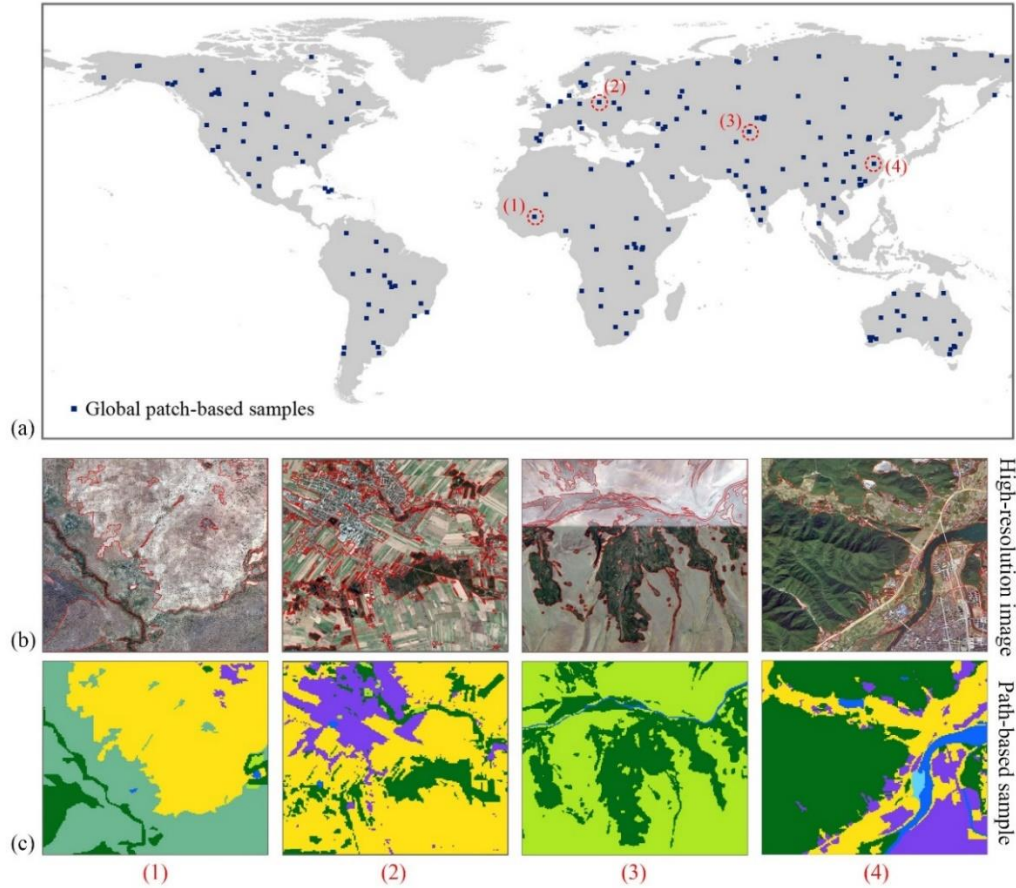
248   **Figure 3. Spatial distribution and selected examples of the global patch-based samples. The location of 5 km**

249   **× 5 km patch-based samples are shown as panel (a), the locations of four selected samples are remarked by**

250   **red dash circles. Panels (b) and (c) illustrate the production of global patch-based samples on manual**

251   **interpretation. The red lines in high-resolution images circa 2015 are results after vectorization using ArcGIS**

252   **10.5 software. Four corresponding patch-based samples are shown as (c).**

253   **3.   Methods**

254   In this study, we proposed a multi-source product fusion method to produce the GLC-2015 map. The

255   procedure mainly comprised the fusion based on the Dempster-Shafer theory of evidence (DSET),

256   accuracy assessment and data inter-comparison (Figure. 4). The basic of this study is the fusion of multi-

257   source GLC products based on DSET. The fusion method was performed at the pixel level and it involves

258   the following three main steps: (1) Construct the basic probability assignment (BPA) function of each

259   pixel that belongs to each LC class considering the accuracy assessment of different GLC products; (2)

calculate the combined probability mass for each class per pixel using the Dempster's rule of combination;

and (3) determine the finally accepted LC class per pixel by a decision rule. Afterwards, pixels with a

determined LC class were integrated to generate a new map. For large-scale or global land cover mapping,

previous researchers divided the study area into a lot of sub-regions and conducted classification in each

sub-region on GEE (Gong et al., 2020; Liu et al., 2020b; Huang et al., 2021; Jin et al., 2022; Zhang et

al., 2021; Zhao et al., 2021). The shape and size of sub-region vary in previous work, such as hexagons

with a side length of 2°, geographical grids with a size of 1°×1°, 3.5°×3.5°, 5°×5°, or 10°×10°. When

deciding on the size of sub-regions, two important factors should be considered. The size of samples in

each sub-region should be sufficient so that the rare land cover classes will not be missed. On the other

hand, it is impossible to implement mapping work at a sub-region as larger as we want due to memory

constraints. To balance the mapping efficiency on the GEE platform and the sufficiency for land cover

classes, we split the world's terrestrial area into 1507 4°×4° geographical grids. The entire framework

was implemented in all 4° × 4° geographical grids on the GEE platform.
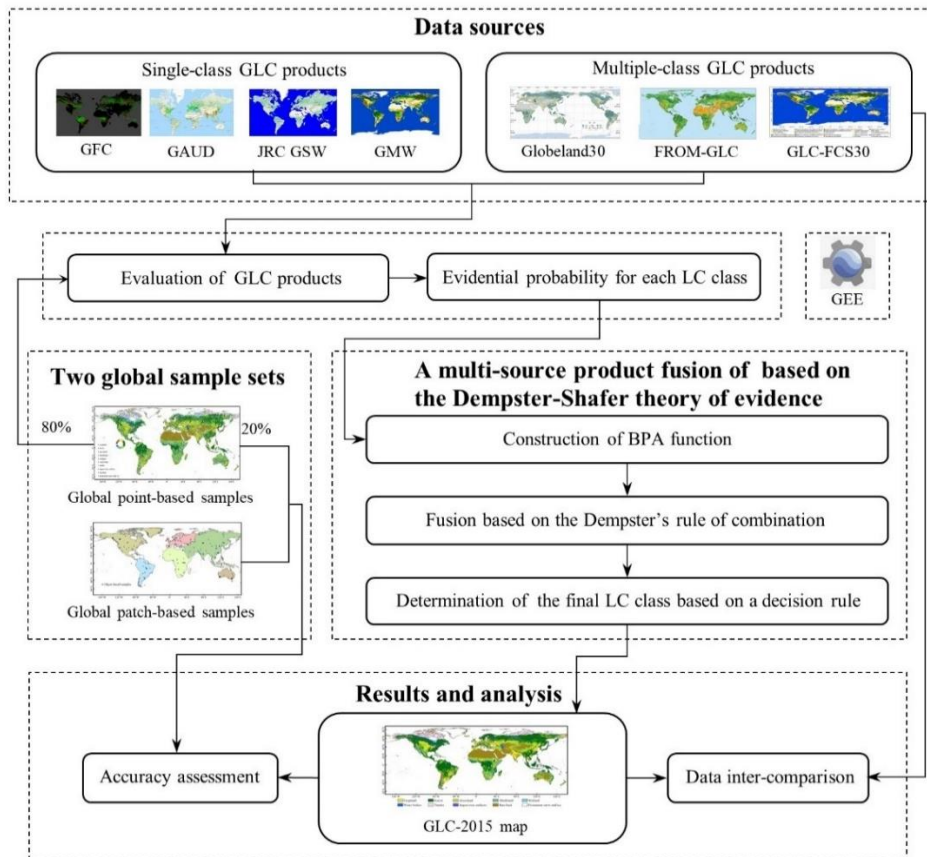
Figure 4. The framework for generating the GLC-2015 map using a multi-source product fusion approach based on DEST.

3.1 Definition of the classification system

Due to the applications for different social needs, the existing GLC products were produced with different classification systems (Table S1). The GlobeLand30 used a simple classification system that only contained 10 first-level classes. Unlike the GlobeLand30, the FROM_GLC and GLC_FCS30 were classified with a two-level classification scheme. Through analysis of these systems, we found that the classification systems are not the same, but they have some agreements. For example, there are both 10 major classes which have the same definition in the GlobeLand30 and FROM_GLC. Additionally, in contrast to the GlobeLand30 and FROM_GLC, the level-0 classification system of the GLC_FCS30 lacks tundra. However, in the level-2 detailed LC classes of the GLC_FCS30, Lichens/mosses has little distinction with tundra. Separately, we selected Lichens/mosses and renamed it as tundra, one of the first-level classes. In this study, we adopted the classification system with 10 LC classes, including cropland, forest, grassland, shrubland, wetland, water bodies, tundra, impervious surfaces, bare land, and permanent snow and ice (Chen et al., 2015), as listed in Table 2. With the discrepancy in the classification system taken into consideration, the 30 level-2 detailed LC classes of GLC_FCS30 were reclassified into 10 major classes according to the classification scheme adopted by our mapping process.

Table 2. Classification system adopted in this paper.

Id	LC class	Definition
10	Cropland	Land areas used for food production and animal feed.
20	Forest	Land areas dominated by trees with tree canopy cover over 30%.
30	Grassland	Land areas dominated by natural grass with a cover over 10%.
40	Shrubland	Land areas dominated by shrubs with a cover over 30%.
50	Wetland	Land areas dominated by wetland plants and water bodies.
60	Water bodies	Land areas covered with accumulated liquid water.
70	Tundra	Land areas dominated by lichen, moss, hardly perennial herb and shrubs in the polar regions.
80	Impervious surfaces	Land areas covered with artificial structures.
90	Bare land	Land areas with scarce vegetation with a cover lower than 10%.
100	Permanent snow and ice	Land areas dominated by permanent snow, glacier and icecap.

3.2 A multi-source product fusion for the GLC-2015 mapping

The DSET is an effective method widely applied for the fusion of multi-source data. To generate a new high-quality GLC map, a multi-source product fusion method using DSET was proposed. In the remainder of the section 3.2, We introduced the overview on the theory and presented the application of DSET in our mapping process.

3.2.1 Dempster-Shafer theory of evidence

The DSET is developed by Dempster and Shafer, which is an extension of Bayesian probability theory. This theory treats information from different data sources as independent evidence and integrated these evidences with no requirements regarding the prior knowledge. In the fusion, we assume a classification process in which all the input data are to be classified into mutually exclusive classes. Let the set Ω of these classes be a frame of discrimination. 2^Ω is the power set of Ω that includes all the classes and their possible unions. We defined the function $\mathrm{m}: 2^\Omega \to [0,1]$ as the basic probability assignment (BPA) function if and only if it satisfies $\mathrm{m}(\Phi) = 0$ and $\sum_{A \subseteq 2^\Omega} \mathrm{m}(A) = 1$ with Ø denotes an empty set. For each class $A \subseteq 2^\Omega$, m(A) is called the basic probability mass which can be computed from the BPA function and represents the degree of support for class A or confidence in class A.

The purpose of fusion is to evaluate and integrate information from multiple sources. In the DSET, these multi-source data are regarded as different evidence and provide different assessments. To generate all the evidences, Dempster-Shafer theory of evidence offers a rule. Suppose $m_i(B_j)$ is the basic probability mass computed from the BPA function for each input data i with $1 \leq \mathrm{i} \leq \mathrm{n}$ for all classes $B_j \in 2^\Omega$. Dempster's rule of combination is provided to calculate a combined probability mass from different evidences. The fusion rules are given in equation (1) and (2).

$$m(C) = \frac{\sum_{B_1 \cap B_2 \dots \cap B_n = C} \prod_{1 \leq i \leq n} m_i(B_j)}{1 - k} \tag{1}$$

$$k = \sum_{B_1 \cap B_2 \dots \cap B_n = \emptyset} \prod_{1 \leq i \leq n} m_i(B_j) \tag{2}$$

Where k represents the basic probability mass associated with conflicts among the sources of evidence. C is the intersection of all classes B_j and carries the joint information from all the input data. After the combination, we took a decision rule to decide the class we finally accept. There are several ways to decide the final class by simply choosing the class with the maximum belief, plausibility, support, or

320   commonality.

321   **3.2.2 Mapping based on DSET**

322   Here, we presented our implementation for the GLC-2015 mapping in the framework of DSET. All the

323   multiple-class and single-class GLC products described in Sect. 2 were selected as input maps to be

324   combined. In the integration of multi-source GLC products, since all the LC classes in our classification

325   system are known, the frame of discrimination was defined to be our classification system:

326    $$\Omega = \left\{ \begin{array}{l} \text{cropland, forest, grassland, shrubland, wetland, water bodies,} \\ \text{tundra, impervious surfaces, bare land, permanent snow and ice} \end{array} \right\} \tag{3}$$

327   The definition of BPA function is the critical point in applying DSET (Rottensteiner et al., 2005).

328   In the fusion, we wanted to achieve a per-pixel classification into one of ten LC classes: cropland, forest,

329   grassland, shrubland, wetland, water bodies, tundra, impervious surfaces, bare land, and permanent snow

330   and ice. For each single-class or multiple-class GLC product, the accuracy for each LC class was

331   calculated and used as evidential probability to construct the BPA. Given that the local accuracy for a

332   4°×4° grid was not able to adequately reflect the actual land cover landscape, especially for the rare LC

333   classes, global accuracy was incorporated into the construction of the BPA to avoid uncertainties from a

334   local point of view. Since assessment based on local samples plays a more critical role in BPA

335   construction for a local grid, higher weight should be assigned to local accuracy. In this case, we chose

336   75% as the weight for local accuracy and 25% for global accuracy as this ratio could achieve robust

337   performance for different regions. Here, we defined the BPA function as follow:

338    $$m_i(T_j) = \frac{PA_{local_{(ij)}} + UA_{local_{(ij)}}}{2} \times 75\% + \frac{PA_{global_{(ij)}} + UA_{global_{(ij)}}}{2} \times 25\% \tag{4}$$

339   Where $m_i(T_j)$ represents the BPA function of evidence source i for the LC class T_j ; $PA_{local_{(ij)}}$,

340    $UA_{local_{(ij)}}$ denote producer's accuracy and user's accuracy of evidence source i for the LC class T_j for

341   each 4° × 4° geographical grid, respectively; $PA_{global_{(ij)}}$, $UA_{global_{(ij)}}$ denote producer's accuracy and

342   user's accuracy of evidence source i for LC class T_j at the global scale.

343   To estimate the exact values of $PA_{local_{(ij)}}$, $UA_{local_{(ij)}}$, $PA_{global_{(ij)}}$ and $UA_{global_{(ij)}}$, we used 80%

344   of the global point-based samples more than 160,000 points derived in Sect 2.3. As soon as we obtained

345   the measurements of $m_i(T_j)$, the combined probability masses $m(T_j)$ were evaluated based on

346   Dempster's rule of combination for each pixel classified as the LC class T_j by fusing BPA values of all

347   the evidence sources:

15

$$m(T_j) = \frac{1}{1-k} \sum_{T_{1j} \cap T_{2j} \dots \cap T_{nj} = T_j} m_i(T_j) \tag{5}$$

348

$$k = \sum_{T_{1j} \cap T_{2j} \dots \cap T_{nj} = \emptyset} m_i(T_j) \tag{6}$$

349

350 Where k represents the basic probability mass associated with conflict; $m_i(T_j)$ represents the basic

351 probability mass of a certain pixel belonging to the LC class T_j from different GLC products.

352   Additionally, a belief measure (Bel) was given to measure the degree of credibility that a pixel

353 labeled as the finally accepted LC class when combining all the available evidences. The belief measure

354 was determined by

$$Bel(T_j) = \sum_{T_{ij} \subseteq T_j} m_i(T_j) \tag{7}$$

355

356   To determine the finally accepted LC class per pixel, we took the rule of maximum combined

357 probability mass as our decision rule and the LC class with the maximum combined probability mass is

358 assigned to the 30 m pixel. Pixels labeled with the LC class were integrated to generate the GLC-2015

359 product.

360 **3.3 Accuracy assessment**

361 To assess the accuracy of the GLC-2015 map, we utilized two validation methods: validation with the

362 global point-based samples and the global patch-based samples. Since the global point-based sample set

363 is distributed evenly across the world and its sample size for each LC class is relatively sufficient and

364 balanced, even for the rare classes, it can provide a representative and credible basis for estimation of the

365 GLC-2015 map globally. Furthermore, we used the global patch-based samples to conduct accuracy

366 assessment from the local landscape scale. Although the global patch-based sample set provide an

367 inadequate sample size for rare LC classes, it can take advantage of the spatial context information and

368 efficiently reflect the actual pattern of the landscape.

369   The error matric was produced to evaluate and analyze the GLC-2015 mapping result. The error

370 matrix is composed of entry A_{ij}, which represents the number of samples with reference LC class j

371 being classified as LC class i. The overall accuracy (OA), kappa coefficient, producer's accuracy (PA),

372 and user's accuracy (UA) were generated from error matric to describe the quality of the GLC-2015 map.

373 They are defined as follows:

$$OA = \frac{\sum_i A_{ii}}{\sum_i \sum_j A_{ij}} \qquad (8)$$

$$P_o = OA \qquad (9)$$

$$P_e = \sum_k \frac{\sum_i A_{ik}}{\sum_i \sum_j A_{ij}} \times \frac{\sum_j A_{kj}}{\sum_i \sum_j A_{ij}} \qquad (10)$$

$$kappa = \frac{P_o - P_e}{1 - P_e} \qquad (11)$$

$$PA^i = \frac{A_{ii}}{\sum_k A_{ki}} \qquad (12)$$

$$UA^i = \frac{A_{ii}}{\sum_k A_{ik}} \qquad (13)$$

Where UA^i and PA^i represent UA and PA of the LC i, respectively; P_o is the agreement between the reference and the classified data; P_e is the hypothetical probability of chance agreement.

3.4 Data inter-comparison

To better reflect the quality of the GLC-2015 map, we intercompared the GLC-2015 map with the GlobeLand30, FROM_GLC and GLC_FCS30. In the accuracy assessment of different products, two global validation sets described earlier were employed.

To figure out whether the GLC-2015 map promotes accuracy in the areas with high classification difficulty and how much the improvement is compared to the other products, we conducted the spatial consistency analysis between the GlobeLand30, FROM_GLC, and GLC_FCS30 and compared the mapping performance of the GLC-2015 with others in the areas of low inconsistency, moderate inconsistency, and high inconsistency. To visually present the spatial consistency between three existing GLC maps, we employed the spatial superposition method to obtain the spatial correspondence pixel-by-pixel between different maps. Based on the times of all the GLC products agreed for the same LC class, the degree of consistency for a pixel was identified as three levels with the agreement value equal to 3, 2, or 1. The areas of low inconsistency were regarded as pixels that classified as the same LC class in all three GLC maps (labeled as 3). The moderate inconsistency areas were regarded as pixels that were consistent in only two GLC maps (labeled as 2). The high inconsistency areas were regarded as pixels that were totally inconsistent in these three GLC maps (labeled as 1). For a visual comparison, all these GLC maps were aggregated to 0.05°, in which the LC class with the largest proportion determined the class in each 0.05° grid.

3.5 Assessment on mapping performance of DSET and other methods

In addition to inter-comparison between the GLC-2015 map and three existing GLC products, we compared the DSET method with two existing commonly used fusion methods, including the majority voting (MV) and spatial correspondence (SC) based on two global validation sets including 20% of the global point-based samples and the whole global patch-based samples. MV is a fusion approach that combines input maps and adopts the LC class favored by the majority of the candidate maps. In the MV method, we compared the GlobeLand30, FROM_GLC, and GLC_FCS30 at each pixel and chose the class that two or three LC products agreed for. For pixels where three LC products were different, the LC class of the product with the highest accuracy was adopted. SC method produces an integrated land cover map by selecting the LC class of the input map that has the highest spatial correspondence with the reference data. In this study, 80% of the global point-based samples were used as the reference data to obtain the SC map of each global LC product. If the class of a product agreed with that of the point-based sample, a value equal to 1 was assigned to that sample. On the contrary, a value equal to 0 was assigned to the sample if the class of the product differed from that of the sample. In each $4° \times 4°$ grid, we used the Kriging method to obtain spatial correspondence maps which have the correspondence value ranging from 0 to 1 for three products. Then, the class of the product with the highest spatial correspondence was chosen for each pixel.

In addition to the comparison between DSET and two other fusion methods, we compared the mapping performance of DSET with Random Forest (RF) which is considered one of the most popular algorithms for land cover mapping. In the land cover classification using the FR classifier, all available Level-2 Tier 1surface reflectance (SR) data of Landsat 8 OLI (Operational Land Imager) sensors from the year 2015 and two adjacent years on GEE was employed. All Landsat images have been atmospherically corrected. The following six bands were used as input features: blue, green, red, NIR, SWIR1, and SWIR2. To improve the mapping performance, several important spectral indices, including DNVI, NDWI, and NDBI were also used as auxiliary data to the RF classifier. The RF classifier was trained on 80% of the global point-based samples since those samples were of high quality after manual visual interpretation of high-resolution images. As the global land cover mapping based on the RF classifier is a tough task, we randomly selected a total of 300 grids with the size of 4° (Figure S1) and applied corresponding local RF classifiers to these grids. Then, the mapping results were validated by

429   the remaining 20% of the global-point samples.

4. Results and discussion

4.1 Mapping result of the GLC-2015 map

Using a multi-source product fusion method based on the DSET, we generated an improved 30m global
land cover map in 2015 (GLC-2015). Figure 5 illustrates the GLC-2015 map. The GLC-2015 map can
accurately describe the spatial distribution of various LC classes. For example, cropland areas are mostly
located in Central America, the region from the Hungarian plain to the Siberian plain, the eastern and
southern parts of China, and the most of India. In addition, forest, which is one of the easily
distinguishable classes from the map, is concentrated in the eastern part of North America, the Amazon
basin of South America, the northern part of Eurasia and the equatorial region of Africa.
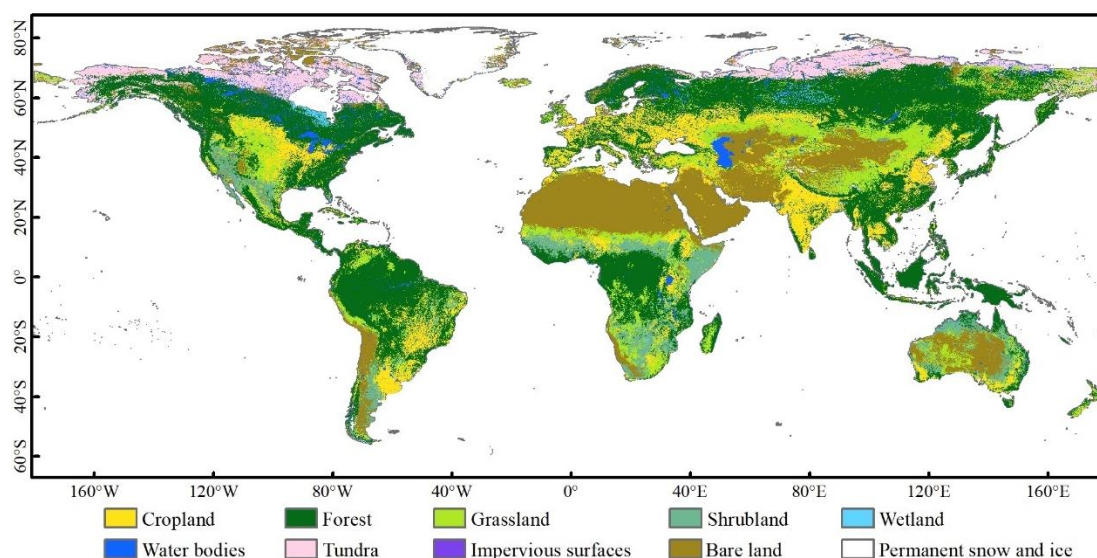
Figure 5. Global land cover map in 2015 with 30 m resolution (GLC-2015).

4.2 Accuracy assessment of the GLC-2015 map

4.2.1 Accuracy assessment with the global point-based samples

The accuracy of the GLC-2015 map was first tested via the global point-based samples, and the results
of assessment are listed in Table 3. The GLC-2015 map achieved an OA of 76.0% and kappa coefficient
of 0.715 at the global scale, demonstrating the good performance of our map. Among all the LC classes,
permanent snow and ice possessed the best mapping performance, with PA and UA achieving 88.1% and
93.2%. The accuracy of water bodies was also high, where PA and UA exceeded 80%. The producer's

accuracy of forest reached 91.7%, while the user's accuracy of that was 78.3%. Grassland, shrubland,

449 and wetland had relatively low accuracy, with PA below 70%. Among them, grassland and shrubland

450 were mainly confused with forest, which might be because these classes are both vegetation, thus causing

451 difficulty in recognition by spectral information. Due to the complex spectral characteristics, wetland is

452 often mixed with vegetation and water bodies (Ludwig et al., 2019). As shown in the confusion matrix,

453 49.53% of wetland was misclassified as vegetation and water bodies.

454 **Table 3. The error metric for the GLC-2015 map based on the global point-based samples.**

|	Cropland	Forest	Grassland	Shrubland	Wetland	Water bodies	Tundra	Impervious surfaces	Bare land	Permanent snow and ice	Total	PA
Cropland	3449	465	418	73	21	53	4	73	96	0	4652	0.741
Forest	173	8888	207	162	92	18	46	46	56	4	9692	0.917
Grassland	65	370	1632	86	29	11	46	41	189	10	2479	0.658
Shrubland	183	539	846	1305	43	32	76	99	514	4	3641	0.358
Wetland	23	587	103	25	659	102	26	14	110	4	1653	0.399
Water bodies	29	107	20	1	86	1937	18	12	51	3	2264	0.856
Tundra	1	269	123	7	0	19	1417	2	268	19	2125	0.667
Impervious surfaces	79	47	13	0	2	15	1	1284	56	1	1498	0.857
Bare land	35	71	330	54	43	104	57	74	4855	40	5663	0.857
Permanent snow and ice	0	11	16	0	4	19	13	1	93	1163	1320	0.881
Total	4073	113543	3708	1713	979	2310	1704	1646	6288	1248	34987	
UA	0.854	0.783	0.440	0.762	0.673	0.839	0.832	0.780	0.772	0.932		
OA					0.760							
Kappa					0.715							

455 The regional accuracies are presented in Figure. 6. The OA of the GLC-2015 ranged from 66.1% to

456 92.7%, and kappa coefficient from 0.552 to 0.813. From the perspective of OA, Water regions lead,

457 followed by Tropical desert, Temperate continental forest, and Polar. These are areas with homogeneous

458 land cover and have low difficulty in mapping. Tropical desert also achieved high OA, but its kappa

459 coefficient was low. Boreal tundra woodland, Tropical dry forest, Tropical shrubland, and Subtropical

460 desert are the regions with low OA. The first one may be related to the high latitudes. The followed two

461   may be because they belong to areas with complicated and mixed LC classes which is not easily classified.

462   The last one may be the consequence of sparse vegetation in desert areas. For the kappa coefficient, the

463   ranking was similar with those for OA, expect for that Tropical desert achieved a low kappa coefficient.
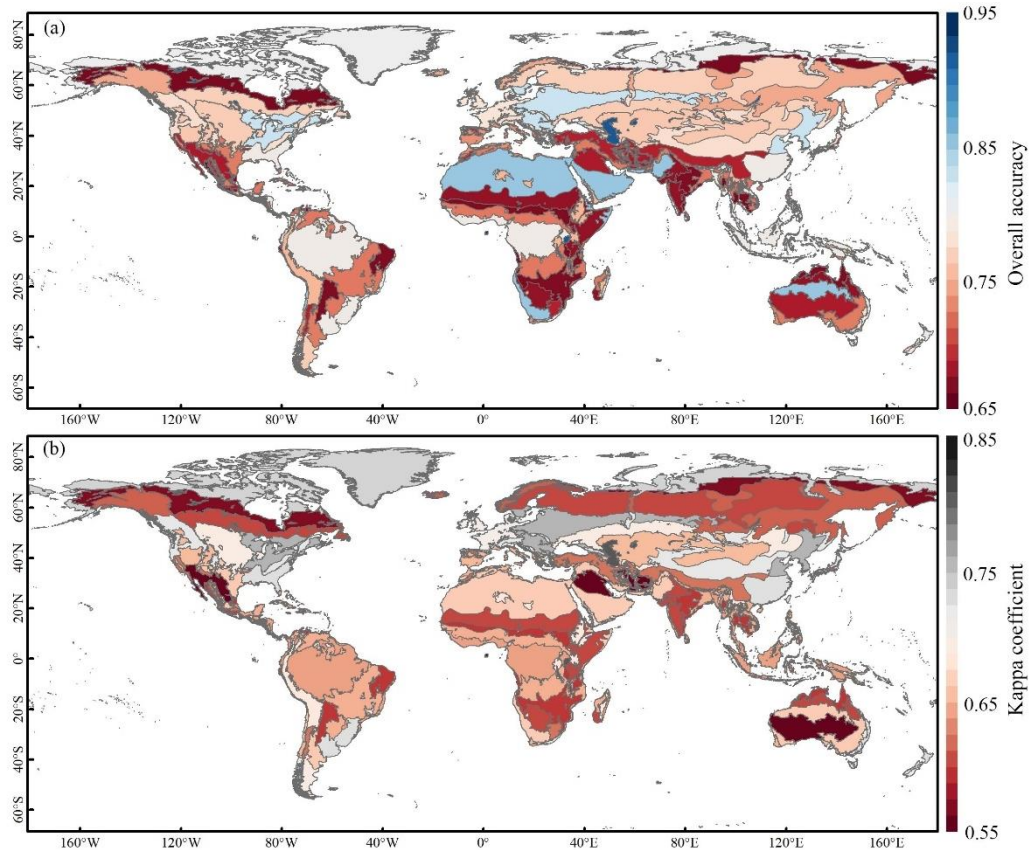
464

465   **Figure 6. Regional accuracy of the GLC-2015 map according to ecoregions. (a)overall accuracy, (b) kappa**

466   **coefficient. The ecoregion boundaries are obtained from the Food and Agriculture Organization of the United**

467   **Nations (FAO).**

468   Figure 7 shows the accuracies of the GLC-2015 map in different ecoregions, where Figure. 7a shows

469   the results of overall accuracy and Figure. 7b of the kappa coefficient. Overall, the mean OA and kappa

470   coefficient were over 60% and 0.50, respectively. However, the OA ranged from 18.8% to 100% and

471   kappa coefficient from 0.15 to 1.00, indicating that the accuracies of mapping fluctuated obviously

472   among different areas. Temperate continental forest and Water regions are the areas with high and stable

473   accuracies. Subtropical desert is the area where accuracies had relatively large fluctuation.
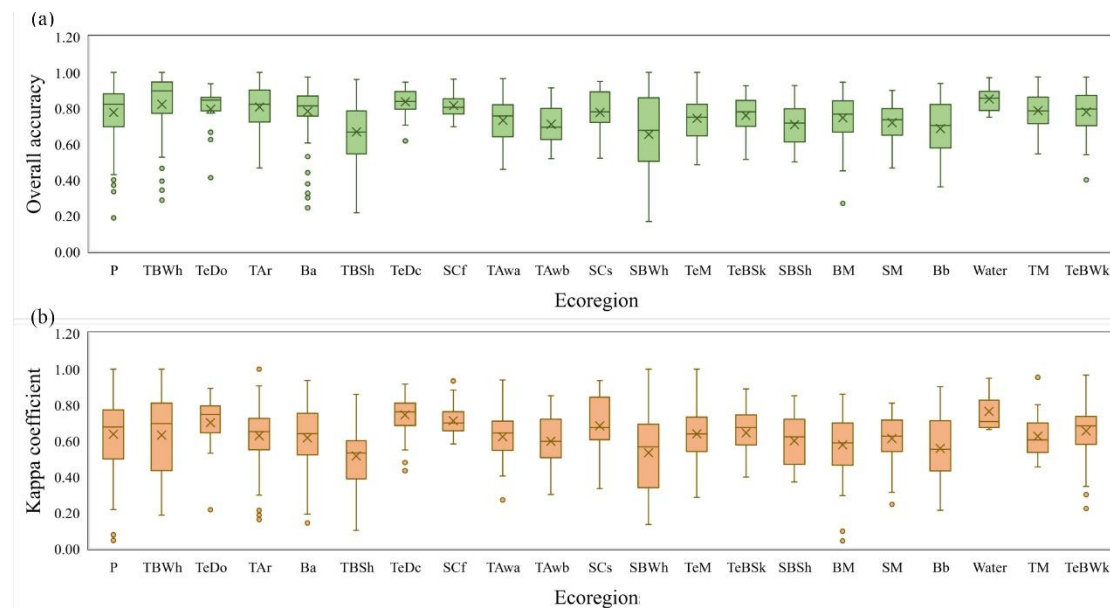
Figure 7. The box-plot of the accuracy for twenty-one ecoregion zones (a) overall accuracy, (b)kappa coefficient. Ecoregion abbreviation and corresponding ecoregion is described in Table S2.

4.2.2 Accuracy assessment with the global patch-based samples

The accuracy assessment of the GLC-2015 map was also conducted with the global patch-based samples. Table 4 summarizes the results for accuracy assessment of each LC class in the GLC-2015 map. From the assessment results, it can be found that the OA of the GLC-2015 map reached 84.4%, which was higher than 76.0% tested with the global point-based samples. The kappa coefficient of the GLC-2015 map was 0.564, which was 0.151 lower than the result calculated with the global point-based samples. In both accuracy assessment results based on two different validation data sets, water bodies, forest, and permanent snow and ice were validated to have high accuracy, and grassland, shrubland, and wetland were validated to have low accuracy. Nevertheless, the ranking of accuracy for each LC class had a slight difference. For example, in assessment based on the global point-based samples, impervious surfaces and permanent snow and ice ranked higher than that based on the global patch-based samples. This may be because a LC map can easily show where one LC class is distributed but hardly describe its actual shape. In addition to the accuracy assessment on a pixel scale, validation on a patch scale is equally important because it can reflect the shape consistency between the GLC-2015 map and the actual landscape, even if the size of global patch-based samples is relatively small. Overall, no matter from the respective of the global point-based samples or the global patch-based samples, the mapping accuracies of the GLC-2015 map are satisfactory.

Table 4. Mapping accuracy via the global patch-based samples for the GLC-2015 map

	Cropland	Forest	Grassland	shrubland	Wetland	Water bodies	Tundra	Impervious surfaces	Bare land	Permanent snow and ice
PA	0.862	0.899	0.626	0.583	0.232	0.939	0.701	0.742	0.757	0.820
UA	0.917	0.814	0.634	0.687	0.647	0.916	0.872	0.722	0.617	0.751
OA						0.844				
Kappa						0.564				

495 **4.3 Inter-comparison with other GLC products**

496 **4.3.1 Inter-comparison based on the global point-based samples**

497 Based on the global point-based samples, the inter-comparison of the GLC-2015 map with the

498 GlobeLand30, FROM_GLC, and GLC_FCS30 were conducted. Since the three products used different

499 classification systems, LC classes were transformed to the classification system we adopted in this paper

500 to achieve consistent accuracy assessment. The accuracy assessment results for all GLC maps are listed

501 in Table 5. It can be found that the GLC-2015 map achieved the highest OA of 76.0% compared with

502 GlobeLand30 of 63.5%, FROM_GLC of 61.3%, and GLC_FCS30 of 63.5%, respectively. The accuracy

503 gap between the GLC-2015 map and other existing ones was 12.5%-14.7%. Also, the GLC-2015 map

504 possessed a better kappa coefficient than other products. For each LC class, the GLC-2015 map

505 outperformed the other three maps in terms of PA in forest, water bodies, impervious surfaces, bare land,

506 and permanent snow and ice. For cropland, grassland, shrub, wetland, and tundra, the GLC-2015 map

507 also exhibited better performance for UA than the GlobeLand30, FROM_GLC and GLC_FCS30. Overall,

508 for the PA or UA, the GLC-2015 map ranked first or second in nearly all LC classes, which demonstrated

509 that the GLC-2015 map had smaller omission and commission errors against the other three products.

Table 5. Mapping accuracy of the GLC products with the global point-based samples.

		Cropland	Forest	Grassland	Shrubland	Wetland	Water bodies	Tundra	Impervious surfaces	Bare land	Permanent snow and ice	OA (Kappa coefficient)
GLC-2015	PA	0.741	0.917	0.658	0.358	0.399	0.856	0.667	0.857	0.857	0.881	0.760
	UA	0.854	0.783	0.440	0.762	0.673	0.839	0.832	0.780	0.772	0.932	(0.715)
Globeland30	PA	0.749	0.712	0.651	0.208	0.508	0.681	0.770	0.681	0.591	0.806	0.635
	UA	0.770	0.805	0.220	0.386	0.521	0.870	0.575	0.790	0.864	0.907	(0.576)
FROM_GLC	PA	0.385	0.694	0.705	0.389	0.347	0.592	0.705	0.751	0.723	0.875	0.613
	UA	0.647	0.862	0.269	0.418	0.282	0.753	0.687	0.646	0.774	0.763	(0.554)
GLC_FCS30	PA	0.744	0.764	0.389	0.354	0.439	0.600	0.227	0.777	0.783	0.712	0.635
	UA	0.596	0.798	0.314	0.385	0.471	0.804	0.688	0.758	0.637	0.948	(0.568)

511   Further quantitative accuracy assessments of different GLC products were performed in 4° × 4°

512 grids using the global point-based samples, and box plots were produced for each product for all grids

513 within different ecoregions, as shown in Figure. 8. It can be found that the GLC-2015 map outperformed

514 other existing products with the best OA and kappa coefficient across different ecoregions. Also, the

515 mean overall accuracy of the GLC-2015 map exceeded 65.0% in all ecoregions, showing the high quality

516 of our mapping result. It is worth noting that the GLC-2015 map showed shorter boxes except in

517 Subtropical mountain systems, Subtropical desert, Subtropical dry forest, Tropical shrubland, and

518 Temperate desert, which means the GLC-2015 map had relatively small fluctuation than other ones. In

519 Tropical dry forest, Tropical shrubland, Subtropical desert, and Boreal tundra woodland, the OA and

520 kappa coefficient of the four products were relatively low. However, the GLC-2015 map exceeded the

521 highest of others by 3.0%-12.9% and greatly improved the mean OA to at least 65.5% in these regions.
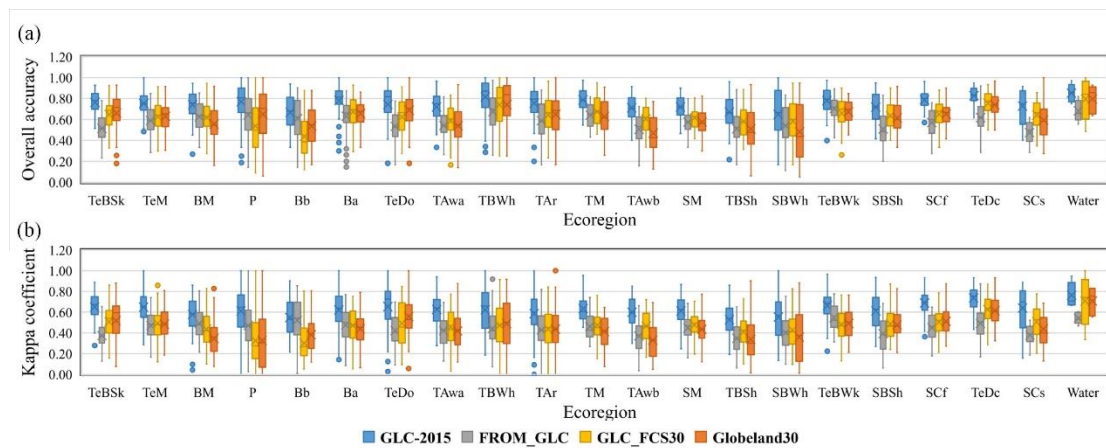
522

525 **4.3.2 Inter-comparison based on the global patch-based samples**

526 Although the global point-based samples are adequate and even across the globe, the distribution of

527 points in each 4° × 4° geographical grid is too sparse to reflect the actual spatial pattern of the landscape.

528 Focusing on LC pattern at the local scale, we also used the global patch-based samples which can provide

529 spatial context information to conduct the accuracy assessment of the GLC-2015 map and compare

530 difference GLC products. Table 6 lists the accuracies of the GLC-2015 map and the other three GLC

531 products. Obviously, the GLC-2015 map achieved the best OA and kappa coefficient among these four

532 GLC maps. The overall accuracy gap between the GLC-2015 product and others was 10.9%-18.5%,

533 which presented a more significant variation compared with the result based on the global point-based

534 samples. In terms of PA and UA, the GLC-2015 map was higher than the other three ones in most LC

535 classes, such as forest, cropland, shrubland, and water bodies. Specifically, all the products had low

536 accuracy for grassland, shrubland, and wetland, similar to that in the accuracy assessment based on the

537 global point-based samples. It is evident that the FROM_GLC had the worst performance in grassland,

538 shrubland, and wetland (as low as 3.2% for UA), implying that the classification method of FROM_GLC

539 is not reliable for these three LC classes.

540 **Table 6. Mapping accuracy of the GLC products with the global patch-based samples**

		Cropland	Forest	Grassland	Shrubland	Wetland	Water bodies	Tundra	Impervious surfaces	Bare land	Permanent snow and ice	OA (Kappa coefficient)
GLC-2015	PA	0.862	0.899	0.626	0.583	0.232	0.939	0.701	0.742	0.757	0.820	0.844
	UA	0.917	0.814	0.634	0.687	0.647	0.916	0.872	0.722	0.617	0.751	(0.564)
Globeland30	PA	0.896	0.698	0.765	0.539	0.455	0.824	0.752	0.643	0.492	0.831	0.735
	UA	0.891	0.906	0.444	0.527	0.157	0.893	0.500	0.703	0.829	0.705	(0.434)
FROM_GLC	PA	0.485	0.714	0.640	0.254	0.032	0.904	0.760	0.506	0.681	0.501	0.659
	UA	0.872	0.809	0.193	0.139	0.186	0.884	0.696	0.808	0.496	0.703	(0.353)
GLC_FCS30	PA	0.865	0.779	0.398	0.565	0.363	0.869	0.051	0.648	0.658	0.742	0.712
	UA	0.857	0.832	0.509	0.330	0.132	0.942	0.573	0.643	0.462	0.752	(0.414)

541 Accuracy assessment was calculated in each patch-based sample, and box plots were produced for

25

each GLC product at the continental scale, as shown in Figure. 9. The GLC-2015 map showed a robust performance in each continent, with the highest OA and kappa coefficient among all the maps. Also, in all continents, the GLC-2015 map had the shortest boxes in terms of OA, which denoted that it had a more minor variation in accuracy at the continental scale. Among four products, the GLC_FCS30 and Globeland30 achieved similar accuracies in most continents. Obviously, the FROM_GLC gave the worst performance across different continents, especially in Oceania, where the OA of most patch-based samples was below 40.0%, namely most of the pixels in Oceania were incorrectly classified. We further compared mapping accuracies for each LC class in different continents (Figure. S2-S3). Since tundra and permanent snow and ice are rare and only existent in certain regions, they were not included in the comparison. As for PA across different continents, the GLC-2015 map outperformed other maps in cropland, forest, water bodies, impervious surfaces, and bare land. As for UA across different continents, the GLC-2015 map outperformed other maps in cropland, grassland, shrubland and wetland, and achieved similar accuracies with the GLC_FCS30 and Globeland30 in forest. Overall, the GLC-2015 map outperformed others regarding mapping accuracy at continental scale. In addition, all GLC products showed significant variation and low mean accuracy in grassland, shrubland, and wetland over most continents, which indicated that the mapping results for these three classes were not reliable enough.
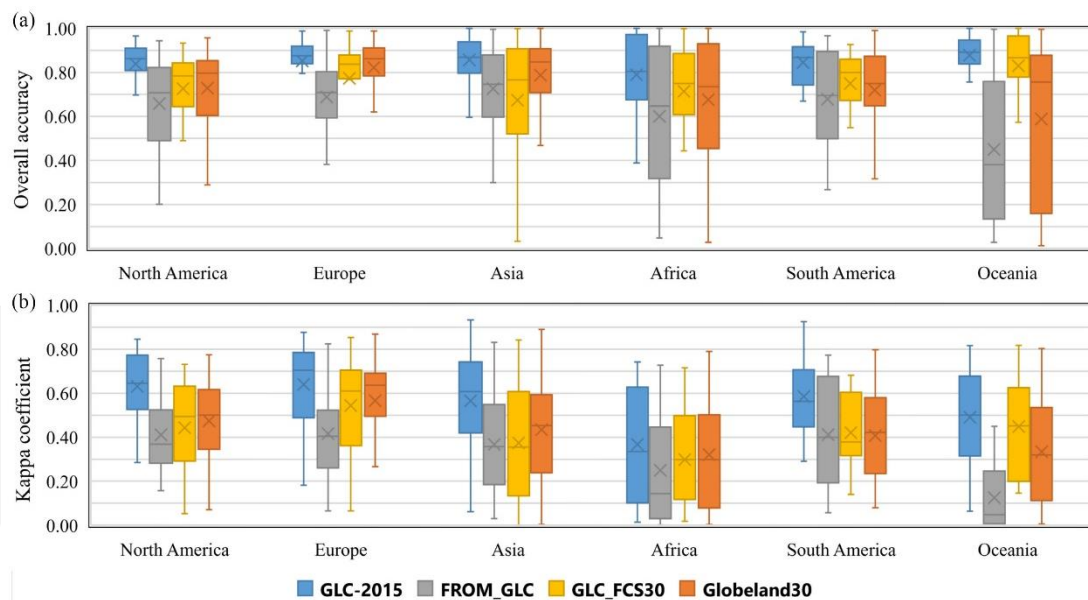
Figure 9. The box-plot of the accuracy for different continents. (a) overall accuracy, (b)kappa coefficient.

Furthermore, to compare the OA of the GLC-2015 map with other GLC products, scatter plots were used to describe the relationship between the overall accuracy of the GLC-2015 map and one other

562   product in each patch-based sample, as displayed in Figure. 10. Most of the points were above the 1:1

563   line, implying that the GLC-2015 map surpassed other GLC products in terms of OA. The distribution

564   of points was more dispersed from the 1:1 line in the plot of the GLC-2015 map against FROM_GLC

565   compared to other plots. It indicated that these two products had a more significant difference, which

566   was also proved in Table 6.
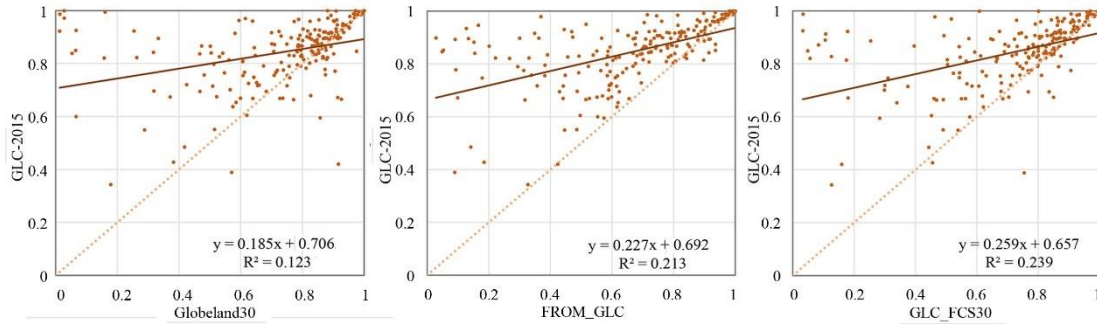
567

568   **Figure 10. Scatter plots between the GLC-2015 map and other products obtained using the global patch-based**

569   **samples.**

570   **4.3.3 Visual inter-comparison at the local scale**

571   Except for quantitative accuracy assessment, we selected six typical geographical tiles covering six

572   continents and different landscape environments to further present the mapping performance of the GLC-

573   2015 map, Globeland30, FROM_GLC, and GLC_FCS30, as shown in Figure. 112. Overall, from a local

574   point of view, the GLC-2015 map tended to be more diverse in LC classes and had better identification

575   performance in various classes. In flattened cropland areas (Figure. 11a and Figure. 11b), the GLC-2015

576   map revealed diverse LC classes and accurately distinguished impervious surfaces; however, the

577   Globeland30 exaggerated the extent of impervious surfaces, and the remaining products failed to

578   delineate impervious surfaces with small size. In addition, the FROM_GLC misclassified some cropland

579   pixels as grassland (Figure. 11a) and had an abnormal "stamp" (Figure.11b). As for mountain areas

580   (Figure. 11c and Figure. 11d), the GLC-2015 map uncovered the spatial pattern of natural and planted

581   forest, cropland, and grassland. There were large confusions between cropland and grassland in the

582   results of the FROM_GLC and GLC_FCS30, and some impervious surfaces and cropland areas were

583   wrongly labeled as bare land by the FROM_GLC. The areas (Figure. 11c), which were classified as forest,

584   were misidentified as cropland and grassland in three other products. For the rainforest areas where a

585   large number of trees were reclaimed for cropland (Figure. 11e), the GLC-2015 map, Globeland30, and

586   GLC_FCS30 had similarities in cropland areas; but the FROM_GLC recognized some reclaimed areas

27

as grassland. Additionally, the GLC-2015 map accurately presented the spatial distribution of impervious

surfaces while other products had omission or commission errors. In the cropland-dominated areas

(Figure. 11f), the GLC-2015 map and Globeland30 showed a higher agreement, and both of them mapped

the undulating areas as grassland. Unlike the aforementioned two products, the FROM_GLC

misclassified large tracts of croplands as grasslands, and the GLC_FCS30 did not capture the grassland

in undulating areas. Figure 11 also shows the belief measure of the fused result in different geographical

tiles. Although it does not directly evaluate the mapping accuracy, it serves as a degree of support for the

hypothesis of an accepted LC class being true, it can still reflect the quality of the GLC-2015 map. Overall,

Bel of the GLC-2015 map exceeded 80% in most areas of each tile, demonstrating the credibility and
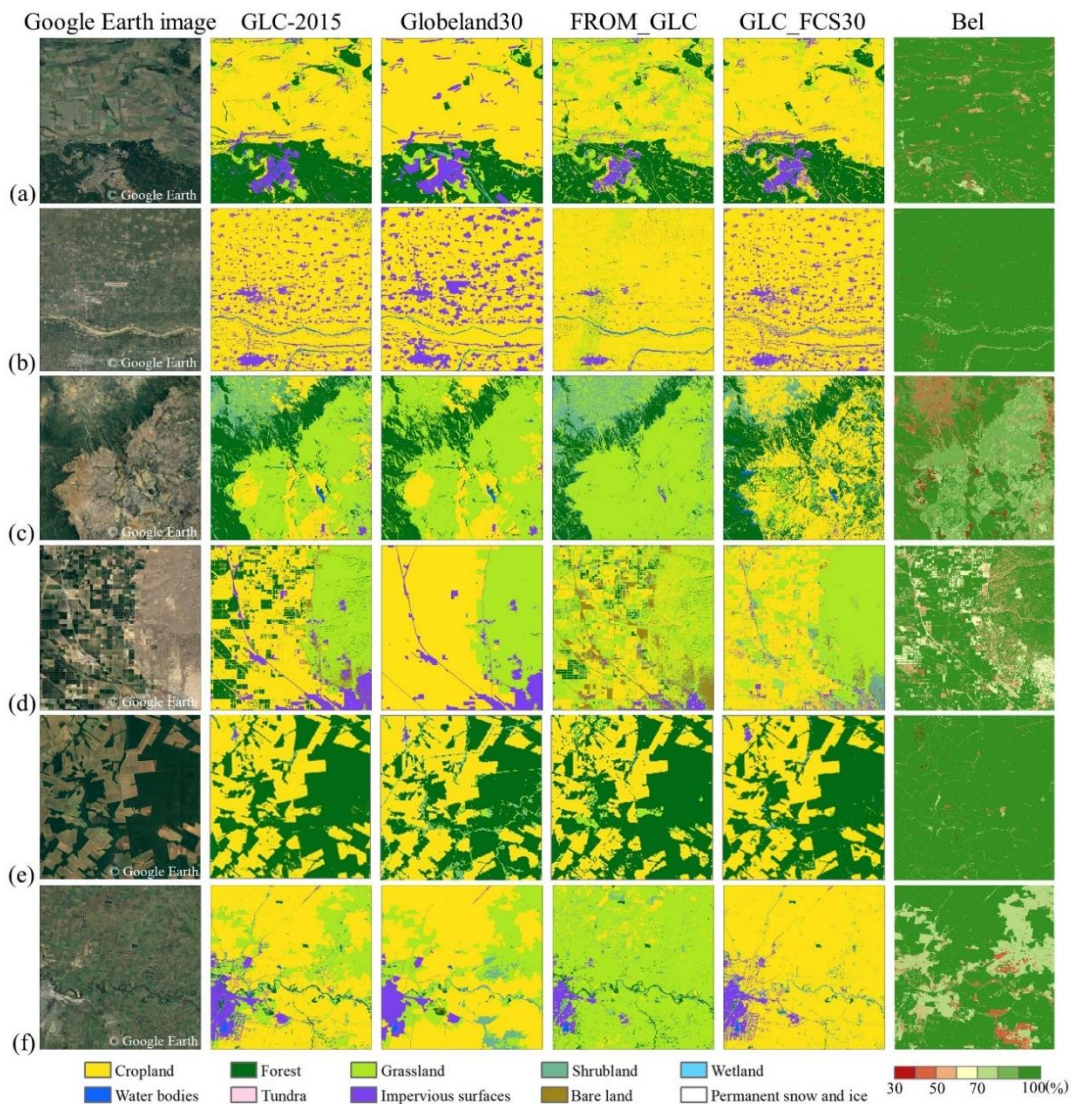
high quality of our mapping result.

Figure 11. Visual comparison between the GLC-2015 map and three other products for different continents.
(a) to (f) are examples for Europe, Asia, Africa, North America, South America, and Oceania, respectively.

4.4 Improvement of the GLC-2015 map compared to other GLC products

The spatial distribution of consistency between three GLC products at the global scale is illustrated in Figure. 12. From the consistency map, we found that areas of low inconsistency mainly corresponded to homogeneous regions with simple LC classes. For example, the northern part of Africa was mainly classified as bare land, the northern part of South America was mainly classified as forest, and the Greenland was classified as permanent snow and ice. On the contrary, areas of high inconsistency were located in regions with complicated LC classes, especially in mixed vegetation regions or sparse vegetation regions, such as northern Asia, South Africa, Sahel region, Australia, northern and southern North America, and eastern and southern South America.
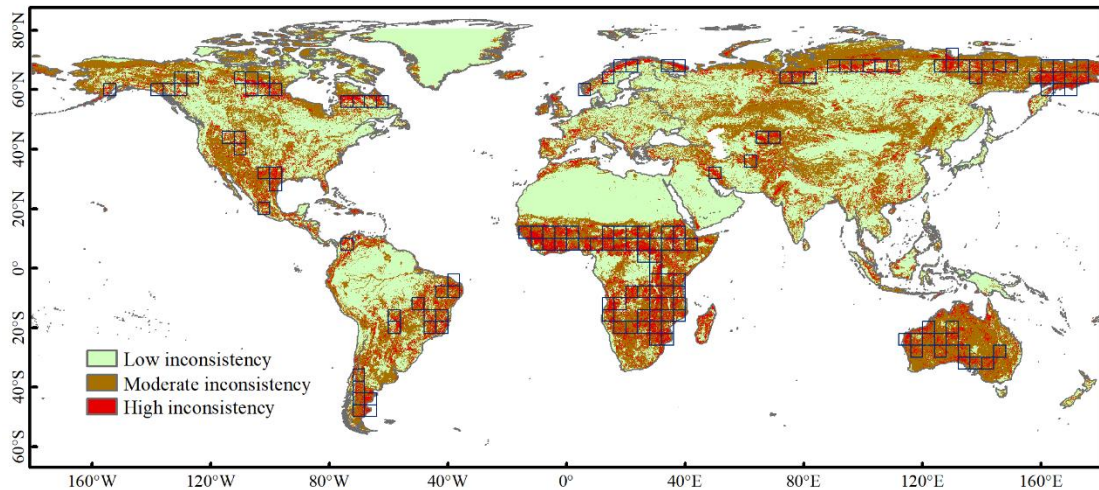
Figure 12. Distribution of consistency between the Globeland30, FROM_GLC, and GLC_FCS30.The blue rectangles are high-inconsistency grids that the area of pixels with value equal to 1 account for more than 20% of the total area.

Based on the global point-based samples, we assessed the accuracies of the GLC-2015 map, Globeland30, FROM_GLC, and GLC_FCS30, in the aforementioned areas of low inconsistency, moderate inconsistency, and high inconsistency, as shown in Table 7. Overall, the GLC-2015 map had the highest accuracies against the other three ones in three areas. For each product, areas of low inconsistency obtained the highest accuracies, followed by areas of moderate inconsistency and then high inconsistency, which demonstrated that inconsistency of the existing products could indicate the quality of maps. In areas of low inconsistency, the overall accuracy gap between the GLC-2015 map and previous ones was as small as 0.2%-1%. However, for areas of moderate and high inconsistency, the comparison accuracy gap expanded to 17.6%-23.2% and 21.0%-25.2%, respectively. It proved the

29

622 overwhelming superiority of the GLC-2015 map over the other three products in the areas of high

623 identification difficulty.

Table 7. Accuracy assessments of the GLC products in three areas.

|	GLC-2015		Globeland30		FROM_GLC		GLC_FCS30	
	OA	Kappa	OA	Kappa	OA	Kappa	OA	Kappa
Areas of low inconsistency	0.939	0.922	0.931	0.912	0.929	0.909	0.937	0.919
Areas of moderate inconsistency	0.717	0.671	0.534	0.467	0.485	0.416	0.541	0.464
Areas of high inconsistency	0.509	0.430	0.285	0.196	0.299	0.212	0.257	0.144

625 We further provided a comparative analysis of three previous GLC products and the GLC-2015 map

626 in areas of high inconsistency. We calculated the area of pixels with a value equal to 1 in 4° × 4° grids.

627 The grids that the area of pixels with a value equal to 1 account for more than 20% of the total area was

628 selected as grids of high inconsistency. Finally, a total number of 147 grids were selected (Figure. 12).

629 To compare the accuracy of the GLC-2015 map and other ones, we utilized scatter plots to represent the

630 relationship between the overall accuracy of one previous product and the GLC-2015 map in each grid

631 of high inconsistency based on the global point-based samples (Figure. 13). Most of the points were

632 above the 1:1line, namely the values of y-axes corresponding to those points were larger than the values

633 of x-axes, which demonstrated that the GLC-2015 map performed better than other GLC products in

634 most grids of high inconsistency. It can be found that the fitting line in each scatter plot had the intercept

635 exceeding 0.39, the slope less than 0.50, and the R^2 less than 0.30, showing that the GLC-2015 map had

636 a large difference with other ones.

637
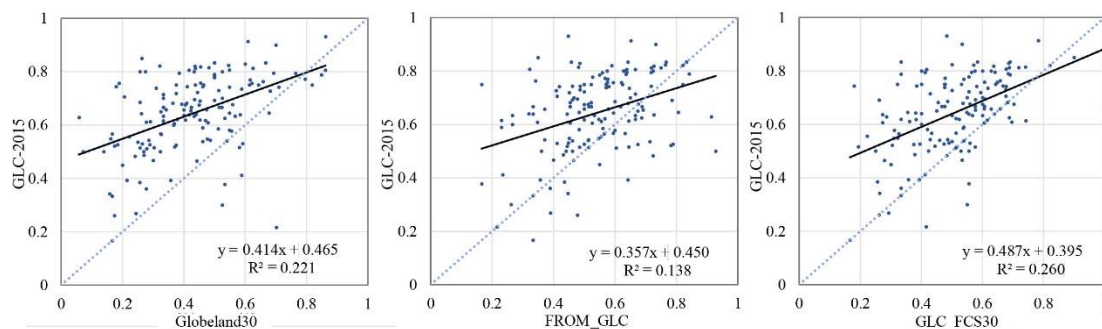
Figure 13. Overall accuracy relationship between the GLC-2015 map and other products in grids of high inconsistency.

640 To intuitively compare the mapping result of the GLC-2015 map and three existing ones in areas of

641 high inconsistency, we focused on visual inspection in various areas based on four 5 km×5km patch-

642 based samples and conducted accuracy statistics, as shown in Figure 14. In the detailed display, it is

643 apparent that three previous products had a large difference in four areas. As can be seen from the four

644 visual cases, the typical confusions between LC classes in areas of high inconsistency were as follows:

645 (1) shrubland was easily misclassified as forest and grassland; (2) cropland, grassland, and shrubland

646 were heavily confused with each other; (3) bare land was likely to be mixed with shrubland and grassland.

647 Except for Figure.14d, the GLC-2015 map surpassed other products in the local accuracy assessment. In

648 Western Australian mulga shrublands (Figure. 14a), the GLC-2015 map and GLC_FCS30 showed similar

649 spatial distribution and shape of bare land and forest, which was consistent with the real landscape. While

650 the Globeland30 wrongly classified bare land as grassland and the FROM_GLC under-classified bare

651 land. As for Zambezian and mopane woodlands (Figure. 14b), the GLC-2015 map performed best with

652 OA reaching 82.6%, followed by the FROM_GLC. In contrast, other products failed to distinguish

653 shrubland from forest. In Western short grasslands (Figure. 14c), the GLC-2015 map had a similar

654 mapping result with the ground truth, with only slight differences in detail. In the results of the

655 Globeland30 and GLC_FCS30, grassland was poorly classified. When it comes to Guinean forest-

656 savanna mosaic (Figure. 14d), the GLC-2015 map and Globeland30 showed high spatial consistency,

657 and both had accurate classification profile for cropland, forest, and impervious surfaces, while other

658 products misidentified cropland as other LC classes.
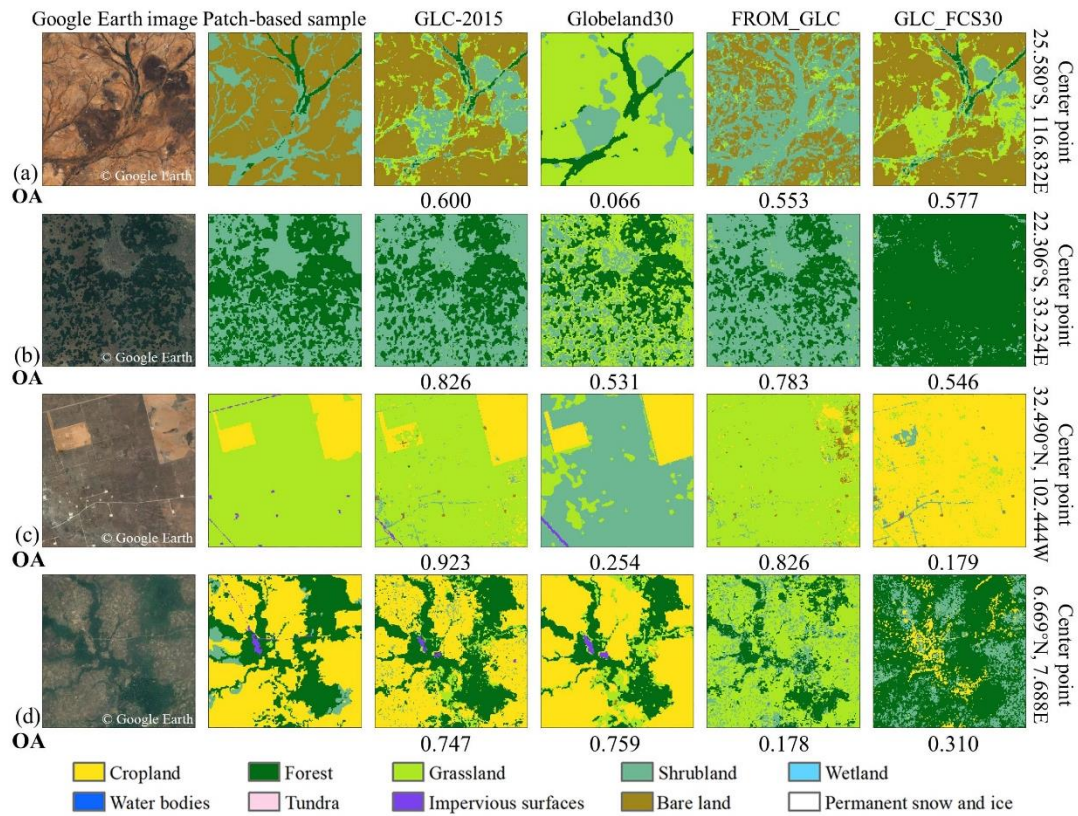
Figure 14. Visual comparison between the GLC-2015 map and three other products based on 5km × 5km patch-based samples and Google Earth images for four areas of high inconsistency (a-d). The OA for each product was calculated by the corresponding patch-based sample.

4.5 Comparison between DSET and other methods

4.5.1 Inter-comparison with other data fusion methods

The accuracy assessments on GLC-2015 obtained by DSET and global mapping results from two other data fusion methods were conducted based on two global validation sample sets. The error matrices with the global point-based samples are shown in Table S3 and S4. The OA of the global land cover classification obtained by the MV and SC was 69.9% and 71.9%, respectively. As shown in Table 3, the OA of the GLC-2015 map obtained by the DSET method was 76.0%, which had an improvement of 6.1% and 4.1% compared to mapping results from the MV and SC. In addition, the GLC-2015 map obtained higher PA and UA for most LC classes.

When evaluating GLC maps obtained by different data fusion approaches using the global patch-based samples, the DSET method obtained the highest OA of 84.4% and kappa coefficient of 0.564, compared with 80.1% and 0.497 for MV, and 71.8% and 0.391 for SC (Table S5). Here, the DSET method achieved an accuracy improvement of 4.3% and 12.6%. Compared to the two other methods, the DSET

676 improved the accuracy for nearly all the LC classes, especially for grassland, shrubland, and wetland.

677 We also compared the overall accuracy relationship between the DSET and other methods. From the

678 scatter plots (Figure 15), we found that the majority of points were above the 1:1 line, implying DSET

679 had better mapping performance than others in most regions across the globe.
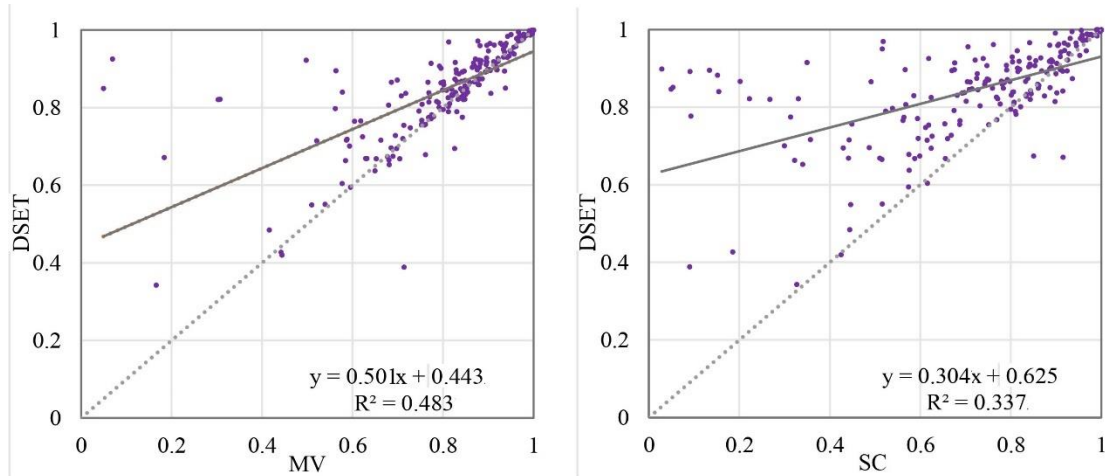
681 **Figure 15. Scatter plots between the DSET and other data fusion methods based on the global patch-based**
682 **samples.**

683 Land cover mapping results from the DSET and other methods were also visually illustrated in six

684 tiles with size of the 0.25° covering different continents, as displayed in Figure S4. Despite that mapping

685 results from the DSET and MV depicted similar spatial distribution of LC classes in all tiles except the

686 tile in North America, the DSET more accurately delineated the impervious surfaces of small size which

687 scattered in cropland-dominated (Figure S4a) or arid areas (Figure S4c). Notably, the mapping results

688 from the SC method presented significant differences from that obtained by the DSET and MV. For

689 example, the SC method failed to capture scattered rural residential areas (Figure S4b) and misclassified

690 grassland as cropland (Figure S4d). Overall, the DSET method possessed better recognition performance

691 in various LC classes than the other two methods.

692 In summary, from the respective of both two global validation sets, the LC map from DSET (GLC-

693 2015) obtained higher OA and performed better in identifying different classes related to those from two

694 others, which demonstrated that the DSET method we adopted is robust to generate a new LC map from

695 the existing products. Especially, the OA of the MV and SC was also higher than the GlobeLand30,

696 FROM_GLC, and GLC_FCS30, confirming that higher accuracy could be achieved by integrating

697 various LC maps.

698 **4.5.2 Inter-comparison with the Random Forest**

699 Based on the validation data from 20% of the global point-based samples, we evaluated the quality of

700 the GLC-2015 map obtained by the DSET method and mapping results classified by the RF classifier for

701 a total of 300 grids. The DSET method obtained an average OA of 77.7% across six continents, while

702 the RF achieved a lower accuracy of 69.8%. From the scatter plots which compared the OA and kappa

703 coefficient between the DSET and RF grid by grid, it was found that the DSET possessed higher accuracy

704 in most grids (Figure S5). Especially, the points were clustered in the upper right corner of the plot

705 (Figure S5a), which indicated that the RF classifier trained with the global point-based samples

706 performed well in those selected grids though it was inferior to the DSET method. Figure S6 shows the

707 OA of the DSET and RF across six continents. We found that the DSET method outperformed RF

708 classifier for each continent. Additionally, the DSET is similar to RF in terms of the ranking of accuracy

709 over the continents. Especially, the mapping results of both two methods presented the lowest accuracy

710 in Oceania. It may be because the selected grids are located in regions with heterogeneous landscape. As

711 for the box plot for the RF classifier, the low hinge exceeded 60.00% in all continents except Oceania,

712 demonstrating the reliability of the RF classifier trained by the global point-based samples. Nevertheless,

713 the performance of the RF classifier was worse than the DSET method. This highlights the feasibility of

714 the DSET method in integrating the existing maps for a better one.

715 **4.6 Advancement and Limitations**

716 To address the problem that current 30m GLC products have great inconsistency in heterogeneous

717 areas and low mapping accuracy for spectral similar LC classes, this study adopted a multi-source

718 product fusion approach based on DSET to create an improved global land cover map (GLC-2015). The

719 results show that the GLC-2015 had good mapping performance with OA reaching 71.5% and 84.4%

720 based on two different validation sets. Compared with those existing products, the GLC-2015 greatly

721 improved the accuracy across the globe, especially in areas of high inconsistency with a significant

722 improvement of 21.0%-25.2%. Compared with other commonly used data fusion methods, the adopted

723 DSET approach provided higher OA and kappa coefficient which showed the benefit of the DEST in

724 integrating various land cover data. No matter from the respective of the global point-based samples or

725 the global patch-based samples, the GLC-2015 showed relatively low accuracy for grassland, shrubland,

726 and wetland compared to other LC classes. Those LC classes are challenging to map at the global scale

727 duo to their spectral similarity to other classes, ambiguous definitions, or variety with regions. However,

728 compared to other existing 30m GLC products, the GLC-2015 map performed better with the PA and OA

729 ranking first or second for grassland, shrubland, and wetland, which indicated the improvement of the

730 GLC-2015 in poorly-mapped LC classes. It was found that the GLC-2015 map had worse performance

731 in areas with more disagreements (Table 7). However, the GLC-2015 map surpassed other products in

732 the areas with different agree of inconsistency. Moreover, the accuracy gap between the GLC-2015 map

733 and other ones in areas of high inconsistency was larger than that in areas with fewer disagreements,

734 implying that the GLC-2015 map provides a more accurate characterization of land cover in poorly-

735 mapped areas. Although the GLC-2015 map was not capable of avoiding all the wrong mapping results

736 caused by the disagreements from the combined GLC products, it proved to be superior to the existing

737 products from the aspects of mapping accuracy for the easily misclassified classes and areas with great

738 inconsistency.

739 Although the GLC-2015 map can evidently improve mapping accuracy in inconsistent areas, there

740 are still some uncertainties. First, we used three multiple-class GLC maps and four single-class GLC

741 maps as the source data for integration. Since those products provided information of land cover at the

742 global scale, classification errors inevitably exist in some specific regions. The multisource product

743 fusion method based on DEST depends highly on the quality of those candidate maps such that the

744 inconsistency between those source maps might lead to incorrect classification. Second, the date time of

745 the GlobeLand30 is different from that of other maps. Because of the five-year time interval, there are

746 changes in land cover, which inevitably distort the fusion results. However, the changed areas are tiny

747 compared to the world's terrestrial area. The uncertainties caused by the LC changes are minor than those

748 from classification errors. In addition, the global point-based samples were used to evaluate the reliability

749 of each product. The accuracy of GlobeLand30 was lower than the other products for areas with LC

750 changes. In this case, the fusion depended more on other maps to avoid the errors caused by LC changes.

751 Third, there might be geographical accuracy biases from the GLC_FCS30 since it adopted a detailed

752 level-2 classification system only for some areas. In this study, we used sufficient point-based samples

753 to assess the accuracy of different GLC products. Based on the evaluation, LC classes could be selected

754 from other more reliable candidate maps if the GLC_FCS30 provided low accuracy. In this way, the

755   uncertainty brought by GLC_FCS30 can be reduced to some extent.

756   As advocated by researchers that the accuracy of the integrated map is expected to be improved

757   with more high-quality data adopted in the mapping task (Fritz et al., 2011; Huang et al., 2022). Several

758   land cover products which focus on a national scale are more likely to offer higher accuracy because they

759   are produced by experts who have good knowledge of land cover classes nationally. Thus, more reliable

760   national land cover products, such as the National Land Cover Database for the year 2016 (NLCD2016)

761   (Yang et al., 2018) and China's land-use/cover datasets (CLUDs) in 2015 (Liu et al., 2014), can further

762   be integrated by our proposed method to develop a more accurate GLC map.

5. Data availability

764   The improved global land cover map in 2015 with 30 m resolution is available at

765   https://doi.org/10.6084/m9.figshare.21371304.v1 (Li et al., 2022). The GLC-2015 product is organized

766   by a total of 1507 4° × 4° geographical grids in GeoTIFF format across the world's terrestrial area. Each

767   image of the GLC-2015 product is named as "GLC-2015_lon_lat" (lon and lat represent the longitude

768   and latitude and of the grid's lower left corner, respectively).

6. Conclusions

770   GLC information at fine spatial resolution is vital for the global environment and climate studies which

771   can capture most human activity. Resulting from the differences in classification scheme, satellite sensor

772   data, classification algorithms and sampling strategies, the existing GLC products have high

773   inconsistency in some parts of the world, especially in fragmented areas and transition zones. More

774   accurate and reliable data with accuracy improved in areas of high mapping inconsistency is very

775   desirable. In this study, with the help of the GEE platform, we developed the GLC-2015 map by

776   integrating multiple existing GLC maps based on the DSET. The GLC-2015 map can significantly

777   increase the mapping accuracy and possess good recognition performance in various LC classes.

778   The GLC-2015 map was validated by both the global point-based samples and the global patch-

779   based samples. Accuracy assessments show that the GLC-2015 map achieved an OA of 76.0%, a kappa

780   coefficient of 0.715 using a total of 34,987 global point-based samples, and an OA of 84.4%, a kappa

781   coefficient of 0.564 using a total of 201 global patch-based samples. Data inter-comparison indicated

that the GLC-2015 map surpassed other three products both visually and quantitatively, by OA improvement of 12.5%-14.7% validated with the global point-based samples and 10.9%-18.5% with the global patch-based samples. Compared to other products, there are fewer misclassifications in the GLC-2015 map for most LC classes, such as forest, cropland, shrubland, and water bodies. Meanwhile, the GLC-2015 map outperformed others in terms of OA and kappa coefficient across different ecoregions and different continents. Notably, the GLC-2015 map showed great superiority over others by an increment of 0.2%-1.0% in overall accuracy for areas of low inconsistency, 17.6%-23.2% for areas of moderate inconsistency, and 21.0%-25.2% for areas of high inconsistency. In addition, the mapping results obtained by the DSET surpassed other data fusion methods with OA improvement of 4.1%-6.1% via the global point-based samples and 4.3%-12.6% via the global patch-based samples. Therefore, it can be concluded that the GLC-2015 map is a robust and reliable map that can significantly improve mapping accuracy compared to previous GLC products and mapping results from other common data fusion methods.

Author contributions

XL and XX conceived the research. BL and XX designed and carried out the experiments. QS and DH provided data. BL wrote the original manuscript. XX, HZ and YC reviewed the writing.

Competing interests

The authors declare that they have no conflict of interest.

References

Ban, Y., Gong, P., and Giri, C.: Global land cover mapping using Earth observation satellite data: Recent

807   progresses   and   challenges,   ISPRS   J.   Photogramm.   Remote   Sens.,   103,   1-6,
808   https://doi.org/10.1016/j.isprsjprs.2015.01.001, 2015.

809   Bartholomé, E. and Belward, A. S.: GLC2000: A new approach to global land cover mapping from Earth
810   observation data, Int. J. Remote Sens., 26, 1959-1977, https://doi.org/10.1080/01431160412331291297,
811   2005.

812   Bounoua, L., DeFries, R., Collatz, G. J., Sellers, P., and Khan, H.: Effects of land cover conversion on
813   surface climate, Climatic Change, 52, 29-64, https://doi.org/10.1023/A:1013051420309, 2002.

814   Bunting, P., Rosenqvist, A., Lucas, R. M., Rebelo, L.-M., Hilarides, L., Thomas, N., Hardy, A., Itoh, T.,
815   Shimada, M., and Finlayson, C. M.: The Global Mangrove Watch—A new 2010 global baseline of
816   mangrove extent, Remote Sen., 10, https://doi.org/10.3390/rs10101669, 2018.

817   Chapin, F. S. I., Zavaleta, E. S., Eviner, V. T., Naylor, R. L., Vitousek, P. M., Reynolds, H. L., Hooper,
818   D. U., Lavorel, S., Sala, O. E., Hobbie, S. E., Mack, M. C., and Díaz, S.: Consequences of changing
819   biodiversity, Nature, 405, 234-242, https://doi.org/10.1038/35012241, 2000.

820   Chen, J., Chen, J., Liao, A., Cao, X., Chen, L., Chen, X., He, C., Han, G., Peng, S., Lu, M., Zhang, W.,
821   Tong, X., and Mills, J.: Global land cover mapping at 30m resolution: A POK-based operational approach,
822   ISPRS J. Photogramm. Remote Sens., 103, 7-27, https://doi.org/10.1016/j.isprsjprs.2014.09.002, 2015.

823   Chen, T. M. and Venkataramanan, V.: Dempster-Shafer theory for intrusion detection in ad hoc networks,
824   IEEE Internet computing, 9, 35-41, https://doi.org/10.1109/MIC.2005.123, 2005.

825   Clinton, N., Yu, L., and Gong, P.: Geographic stacking: Decision fusion to increase global land cover
826   map   accuracy,   ISPRS   J.   Photogramm.   Remote   Sens.,   103,   57-65,
827   https://doi.org/10.1016/j.isprsjprs.2015.02.010, 2015.

828   Land Cover CCI: Product User Guide Version 2: https://www.esa-landcover-cci.org/?q=webfm_send/84,
829   last access: 21 January 2022.

830   DeFries, R. S., Houghton, R. A., Hansen, M. C., Field, C. B., Skole, D., and Townshend, J.: Carbon
831   emissions from tropical deforestation and regrowth based on satellite observations for the 1980s and
832   1990s, Proc. Natl. Acad. Sci. U.S.A., 99, 14256, https://doi.org/10.1073/pnas.182560099, 2002.

833   Foley, J. A., DeFries, R., Asner, G. P., Barford, C., Bonan, G., Carpenter, S. R., Chapin, F. S., Coe, M. T.,
834   Daily, G. C., Gibbs, H. K., Helkowski, J. H., Holloway, T., Howard, E. A., Kucharik, C. J., Monfreda,
835   C., Patz, J. A., Prentice, I. C., Ramankutty, N., and Snyder, P. K.: Global Consequences of Land Use,
836   Science, 309, 570-574, https://doi.org/10.1126/science.1111772, 2005.

837   Friedl, M. A., Sulla-Menashe, D., Tan, B., Schneider, A., Ramankutty, N., Sibley, A., and Huang, X.:
838   MODIS Collection 5 global land cover: Algorithm refinements and characterization of new datasets,
839   Remote Sens. Environ., 114, 168-182, https://doi.org/10.1016/j.rse.2009.08.016, 2010.

840   Fritz, S., You, L., Bun, A., See, L., McCallum, I., Schill, C., Perger, C., Liu, J., Hansen, M., and
841   Obersteiner, M.: Cropland for sub-Saharan Africa: A synergistic approach using five land cover data sets,
842   Geophy.   Res. Lett., 38, L04404, https://doi.org/10.1029/2010GL046213, 2011.

843   Gao, Y., Liu, L., Zhang, X., Chen, X., Mi, J., and Xie, S.: Consistency Analysis and Accuracy Assessment
844   of Three Global 30-m Land-Cover Products over the European Union using the LUCAS Dataset, Remote
845   Sen., 12, 3479, https://doi.org/10.3390/rs12213479, 2020.

846   Gengler, S. and Bogaert, P.: Combining land cover products using a minimum divergence and a Bayesian
847   data   fusion   approach,   Int.   J.   Geogr.   Inf.   Sci.   ,   32,   806-826,
848   https://doi.org/10.1080/13658816.2017.1413577, 2018.

849   Giri, C., Zhu, Z., and Reed, B.: A comparative analysis of the Global Land Cover 2000 and MODIS land
850   cover data sets, Remote Sens. Environ., 94, 123-132, https://doi.org/10.1016/j.rse.2004.09.005, 2005.

Giri, C., Pengra, B., Long, J., and Loveland, T. R.: Next generation of global land cover characterization, mapping, and monitoring, Int. J. Appl. Earth Obs. Geoinf., 25, 30-37, https://doi.org/10.1016/j.jag.2013.03.005, 2013.

Gómez, C., White, J. C., and Wulder, M. A.: Optical remotely sensed time series data for land cover classification: A review, ISPRS J. Photogramm. Remote Sens., 116, 55-72, https://doi.org/10.1016/j.isprsjprs.2016.03.008, 2016.

Gong, P.: Remote sensing of environmental change over China: A review, Sci. Bull., 57, 2793-2801, https://doi.org/10.1007/s11434-012-5268-y, 2012.

Gong, P., Yu, L., Li, C., Wang, J., Liang, L., Li, X., Ji, L., Bai, Y., Cheng, Y., and Zhu, Z.: A new research paradigm for global land cover mapping, Ann. GIS, 22, 87-102, https://doi.org/10.1080/19475683.2016.1164247, 2016.

Gong, P., Li, X., Wang, J., Bai, Y., Chen, B., Hu, T., Liu, X., Xu, B., Yang, J., Zhang, W., and Zhou, Y.: Annual maps of global artificial impervious area (GAIA) between 1985 and 2018, Remote Sens. Environ., 236, 111510, https://doi.org/10.1016/j.rse.2019.111510, 2020.

Gong, P., Wang, J., Yu, L., Zhao, Y., Zhao, Y., Liang, L., Niu, Z., Huang, X., Fu, H., Liu, S., Li, C., Li, X., Fu, W., Liu, C., Xu, Y., Wang, X., Cheng, Q., Hu, L., Yao, W., Zhang, H., Zhu, P., Zhao, Z., Zhang, H., Zheng, Y., Ji, L., Zhang, Y., Chen, H., Yan, A., Guo, J., Yu, L., Wang, L., Liu, X., Shi, T., Zhu, M., Chen, Y., Yang, G., Tang, P., Xu, B., Giri, C., Clinton, N., Zhu, Z., Chen, J., and Chen, J.: Finer resolution observation and monitoring of global land cover: first mapping results with Landsat TM and ETM+ data, Int. J. Remote Sens., 34, 2607-2654, https://doi.org/10.1080/01431161.2012.748992, 2013.

Grekousis, G., Mountrakis, G., and Kavouras, M.: An overview of 21 global and 43 regional land-cover mapping products, Int. J. Remote Sens., 36, 5309-5335, https://doi.org/10.1080/01431161.2015.1093195, 2015.

Grimm, N. B., Faeth, S. H., Golubiewski, N. E., Redman, C. L., Wu, J., Bai, X., and Briggs, J. M.: Global change and the ecology of cities, Science, 319, 756-760, https://doi.org/10.1126/science.1150195, 2008.

Hansen, M. C., Defries, R. S., Townshend, J. R. G., and Sohlberg, R.: Global land cover classification at 1 km spatial resolution using a classification tree approach, Int. J. Remote Sens., 21, 1331-1364, https://doi.org/10.1080/014311600210209, 2000.

Hansen, M. C., Potapov, P. V., Moore, R., Hancher, M., Turubanova, S. A., Tyukavina, A., Thau, D., Stehman, S. V., Goetz, S. J., Loveland, T. R., Kommareddy, A., Egorov, A., Chini, L., Justice, C. O., and Townshend, J. R. G.: High-resolution global maps of 21st-century forest cover change, Science, 342, 850-853, https://doi.org/10.1126/science.1244693, 2013.

Herold, M., Mayaux, P., Woodcock, C. E., Baccini, A., and Schmullius, C.: Some challenges in global land cover mapping: An assessment of agreement and accuracy in existing 1 km datasets, Remote Sens. Environ., 112, 2538-2556, https://doi.org/10.1016/j.rse.2007.11.013, 2008.

Huang, A., Shen, R., Li, Y., Han, H., Di, W., and Hagan, D. F.: A methodology to generate integrated land cover data for land surface model by improving Dempster-Shafer theory, Remote Sen., 14, 972, https://10.3390/rs14040972, 2022.

Huang, X., Li, J., Yang, J., Zhang, Z., Li, D., and Liu, X.: 30 m global impervious surface area dynamics and urban expansion pattern observed by Landsat satellites: From 1972 to 2019, Sci. China Earth Sci., 64, 1922-1933, https://10.1007/s11430-020-9797-9, 2021.

Iwao, K., Nasahara, K. N., Kinoshita, T., Yamagata, Y., Patton, D., and Tsuchida, S.: Creation of new global land cover map with map integration, J. Geogr. Inf. Syst., 3, 160-165, https://doi.org/10.4236/jgis.2011.32013, 2011.

Jin, Q., Xu, E., and Zhang, X.: A fusion method for multisource land cover products based on superpixels and statistical extraction for enhancing resolution and improving accuracy, Remote Sen., 14, 1676, https://doi.org/10.3390/rs14071676, 2022.

Jung, M., Henkel, K., Herold, M., and Churkina, G.: Exploiting synergies of global land cover products for carbon cycle modeling, Remote Sens. Environ., 101, 534-553, https://doi.org/10.1016/j.rse.2006.01.020, 2006.

Kang, J., Wang, Z., Sui, L., Yang, X., Ma, Y., and Wang, J.: Consistency Analysis of Remote Sensing Land Cover Products in the Tropical Rainforest Climate Region: A Case Study of Indonesia, Remote Sen., 12, 1410, https://doi.org/10.3390/rs12091410, 2020.

Li, B., Xu, X., Liu, X., Shi, Q., Zhuang, H., Cai, Y., and He, D.: An improved global land cover mapping in 2015 with 30 m resolution (GLC-2015) based on a multi-source product fusion approach. [dataset], https://doi.org/10.6084/m9.figshare.21371304.v1, 2022.

Li, C., Gong, P., Wang, J., Zhu, Z., Biging, G. S., Yuan, C., Hu, T., Zhang, H., Wang, Q., Li, X., Liu, X., Xu, Y., Guo, J., Liu, C., Hackman, K. O., Zhang, M., Cheng, Y., Yu, L., Yang, J., Huang, H., and Clinton, N.: The first all-season sample set for mapping global land cover with Landsat-8 data, Sci. Bull., 62, 508-515, https://doi.org/10.1016/j.scib.2017.03.011, 2017.

Liu, H., Gong, P., Wang, J., Clinton, N., Bai, Y., and Liang, S.: Annual dynamics of global land cover and its long-term changes from 1982 to 2015, Earth Syst. Sci. Data, 12, 1217-1243, https://doi.org/10.5194/essd-12-1217-2020, 2020a.

Liu, H., Gong, P., Wang, J., Wang, X., Ning, G., and Xu, B.: Production of global daily seamless data cubes and quantification of global land cover change from 1985 to 2020 - iMap World 1.0, Remote Sens. Environ., 258, 112364, https://doi.org/10.1016/j.rse.2021.112364, 2021a.

Liu, J., Kuang, W., Zhang, Z., Xu, X., Qin, Y., Ning, J., Zhou, W., Zhang, S., Li, R., Yan, C., Wu, S., Shi, X., Jiang, N., Yu, D., Pan, X., and Chi, W.: Spatiotemporal characteristics, patterns and causes of land use changes in China since the late 1980s, Dili Xuebao/Acta Geogr. Sin., 69, 3-14, https://doi.org/10.11821/dlxb201401001, 2014.

Liu, K. and Xu, E.: Fusion andcorrection of multi-source land cover products based on spatial detection and uncertainty reasoning methods in Central Asia, Remote Sen., 13, 244, https://doi.org/10.3390/rs13020244, 2021.

Liu, L., Zhang, X., Gao, Y., Chen, X., Shuai, X., and Mi, J.: Finer-resolution mapping of global land cover: Recent developments, consistency analysis, and prospects, Journal of Remote Sensing, 2021, 5289697, https://doi.org/10.34133/2021/5289697, 2021b.

Liu, X., Huang, Y., Xu, X., Li, X., Li, X., Ciais, P., Lin, P., Gong, K., Ziegler, A. D., Chen, A., Gong, P., Chen, J., Hu, G., Chen, Y., Wang, S., Wu, Q., Huang, K., Estes, L., and Zeng, Z.: High-spatiotemporal-resolution mapping of global urban change from 1985 to 2015, Nature Sustainability, 3, 564-570, https://doi.org/10.1038/s41893-020-0521-x, 2020b.

Loveland, T. R., Reed, B. C., Brown, J. F., Ohlen, D. O., Zhu, Z., Yang, L., and Merchant, J. W.: Development of a global land cover characteristics database and IGBP DISCover from 1 km AVHRR data, Int. J. Remote Sens., 21, 1303-1330, https://doi.org/10.1080/014311600210191, 2000.

Ludwig, C., Walli, A., Schleicher, C., Weichselbaum, J., and Riffler, M.: A highly automated algorithm for wetland detection using multi-temporal optical satellite data, Remote Sens. Environ., 224, 333-351, https://doi.org/10.1016/j.rse.2019.01.017, 2019.

Mayaux, P., Bartholomé, E., Fritz, S., and Belward, A.: A New Land-Cover Map of Africa for the Year 2000, J. Biogeogr., 31, 861-877, https://doi.org/10.1111/j.1365-2699.2004.01073.x, 2004.

McCallum, I., Obersteiner, M., Nilsson, S., and Shvidenko, A.: A spatial comparison of four satellite derived 1km global land cover datasets, Int. J. Appl. Earth Obs. Geoinf., 8, 246-255, https://doi.org/10.1016/j.jag.2005.12.002, 2006.

Meyer, M. F., Labou, S. G., Cramer, A. N., Brousil, M. R., and Luff, B. T.: The global lake area, climate, and population dataset, Sci. Data, 7, 174, 10.1038/s41597-020-0517-4, 2020.

Moody, A. and Woodcock, C.: Scale-dependent errors in the estimation of land-cover proportions: Implications for global land-cover datasets, Photogramm. Eng. Rem. S., 60, 585-594, 1994.

Pekel, J.-F., Cottam, A., Gorelick, N., and Belward, A. S.: High-resolution mapping of global surface water and its long-term changes, Nature, 540, 418-422, https://doi.org/10.1038/nature20584, 2016.

Pengra, B. W., Stehman, S. V., Horton, J. A., Dockter, D. J., Schroeder, T. A., Yang, Z., Cohen, W. B., Healey, S. P., and Loveland, T. R.: Quality control and assessment of interpreter consistency of annual land cover reference data in an operational national monitoring program, Remote Sens. Environ., 238, 111261, https://doi.org/10.1016/j.rse.2019.111261, 2020.

Razi, S., Karami Mollaei, M. R., and Ghasemi, J.: A novel method for classification of BCI multi-class motor imagery task based on Dempster–Shafer theory, Inf. Sci., 484, 14-26, https://doi.org/10.1016/j.ins.2019.01.053, 2019.

Rottensteiner, F., Trinder, J. C., Clode, S., and Kubik, K.: Using the Dempster-Shafer method for the fusion of LIDAR data and multi-spectral images for building detection, Inform. Fusion., 6, 283-300, https://doi.org/10.1016/j.inffus.2004.06.004, 2005.

Running, S. W.: Ecosystem disturbance, carbon, and climate, Science, 321, 652-653, https://doi.org/10.1126/science.1159607, 2008.

Schewe, J., Gosling, S. N., Reyer, C., Zhao, F., Ciais, P., Elliott, J., Francois, L., Huber, V., Lotze, H. K., Seneviratne, S. I., van Vliet, M. T. H., Vautard, R., Wada, Y., Breuer, L., Büchner, M., Carozza, D. A., Chang, J., Coll, M., Deryng, D., de Wit, A., Eddy, T. D., Folberth, C., Frieler, K., Friend, A. D., Gerten, D., Gudmundsson, L., Hanasaki, N., Ito, A., Khabarov, N., Kim, H., Lawrence, P., Morfopoulos, C., Müller, C., Müller Schmied, H., Orth, R., Ostberg, S., Pokhrel, Y., Pugh, T. A. M., Sakurai, G., Satoh, Y., Schmid, E., Stacke, T., Steenbeek, J., Steinkamp, J., Tang, Q., Tian, H., Tittensor, D. P., Volkholz, J., Wang, X., and Warszawski, L.: State-of-the-art global models underestimate impacts from climate extremes, Nat. Commun., 10, 1005, https://doi.org/10.1038/s41467-019-08745-6, 2019.

See, L., Schepaschenko, D., Lesiv, M., McCallum, I., Fritz, S., Comber, A., Perger, C., Schill, C., Zhao, Y., Maus, V., Siraj, M. A., Albrecht, F., Cipriani, A., Vakolyuk, M. y., Garcia, A., Rabia, A. H., Singha, K., Marcarini, A. A., Kattenborn, T., Hazarika, R., Schepaschenko, M., van der Velde, M., Kraxner, F., and Obersteiner, M.: Building a hybrid land cover map with crowdsourcing and geographically weighted regression, ISPRS J. Photogramm. Remote Sens., 103, 48-56, https://doi.org/10.1016/j.isprsjprs.2014.06.016, 2015.

Song, X., Hansen, M. C., Stehman, S. V., Potapov, P. V., Tyukavina, A., Vermote, E. F., and Townshend, J. R.: Global land change from 1982 to 2016, Nature, 560, 639-643, https://doi.org/10.1038/s41586-018-0411-9, 2018.

Sun, B., Chen, X., and Zhou, Q.: Uncertainty assessment of GlobeLand30 land cover data set over central Asia, Int. Arch. Photogramm. Remote Sens. Spat. Inf. Sci., 41, 1313, https://doi.org/10.5194/isprs-archives-XLI-B8-1313-2016, 2016.

Verburg, P. H., Neumann, K., and Nol, L.: Challenges in using land use and land cover data for global change studies, Glob. Change Biol., 17, 974-989, https://doi.org/10.1111/j.1365-2486.2010.02307.x, 2011.

Verburg, P. H., Mertz, O., Erb, K.-H., Haberl, H., and Wu, W.: Land system change and food security: towards multi-scale land system solutions, Curr. Opin. Environ. Sustain., 5, 494-502, https://doi.org/10.1016/j.cosust.2013.07.003, 2013.

Xu, G., Zhang, H., Chen, B., Zhang, H., Yan, J., Chen, J., Che, M., Lin, X., and Dou, X.: A Bayesian based method to generate a synergetic land-cover map from existing land-cover products., https://doi.org/10.3390/rs606558910.3390/rs6065589, 2014.

Yang, J. and Huang, X.: The 30 m annual land cover dataset and its dynamics in China from 1990 to 2019, Earth Syst. Sci. Data, 13, 3907-3925, https://doi.org/10.5194/essd-13-3907-2021, 2021.

Yang, J., Gong, P., Fu, R., Zhang, M., Chen, J., Liang, S., Xu, B., Shi, J., and Dickinson, R.: The role of satellite remote sensing in climate change studies, Nat. Clim. Chang., 3, 875-883, https://doi.org/10.1038/nclimate1908, 2013.

Yang, L., Jin, S., Danielson, P., Homer, C., Gass, L., Bender, S. M., Case, A., Costello, C., Dewitz, J., Fry, J., Funk, M., Granneman, B., Liknes, G. C., Rigge, M., and Xian, G.: A new generation of the United States National Land Cover Database: Requirements, research priorities, design, and implementation strategies, ISPRS J. Photogramm. Remote Sens., 146, 108-123, https://doi.org/10.1016/j.isprsjprs.2018.09.006, 2018.

Yang, Y., Xiao, P., Feng, X., and Li, H.: Accuracy assessment of seven global land cover datasets over China, ISPRS J. Photogramm. Remote Sens., 125, 156-173, https://doi.org/10.1016/j.isprsjprs.2017.01.016, 2017.

Zhang, C., Dong, J., and Ge, Q.: Quantifying the accuracies of six 30-m cropland datasets over China: A comparison and evaluation analysis, Comput. Electron. Agric., 197, 106946, https://doi.org/10.1016/j.compag.2022.106946, 2022.

Zhang, X., Liu, L., Chen, X., Gao, Y., Xie, S., and Mi, J.: GLC_FCS30: global land-cover product with fine classification system at 30 m using time-series Landsat imagery, Earth Syst. Sci. Data, 13, 2753-2776, https://doi.org/10.5194/essd-13-2753-2021, 2021.

Zhao, J., Yu, L., Liu, H., Huang, H., Wang, J., and Gong, P.: Towards an open and synergistic framework for mapping global land cover, PeerJ, 9, e11877, https://doi.org/10.7717/peerj.11877, 2021.